

We are IntechOpen, the world's leading publisher of Open Access books Built by scientists, for scientists

6,900

Open access books available

186,000

International authors and editors

200M

Downloads

Our authors are among the

154

Countries delivered to

TOP 1%

most cited scientists

12.2%

Contributors from top 500 universities



WEB OF SCIENCE™

Selection of our books indexed in the Book Citation Index
in Web of Science™ Core Collection (BKCI)

Interested in publishing with us?
Contact book.department@intechopen.com

Numbers displayed above are based on latest data collected.
For more information visit www.intechopen.com



Investigation of Structural, Magnetic and Electrical Properties of Chromium Substituted Nickel Ceramic Nanopowders

Rapolu Sridhar, D. Ravinder, J. Laxman Naik, K. Vijaya Kumar, N. Maramu and S. Katlakunta

Abstract

Nano-ceramic of $\text{NiCr}_x\text{Fe}_{2-x}\text{O}_4$ ($0.1 \leq x \leq 1.0$) ferrites were synthesized by citrate-gel auto combustion method. The structural parameter such as lattice parameter, X-ray density, bulk density and porosity variations with Cr doping were studied. The average crystallite size is in the range 8.5–10.5 nm. The surface morphology and elemental analysis was studied with SEM (EDAX) spectrum and the structural information analyzed with FTIR spectra. Magnetic properties were discussed with Cr^{3+} ion concentration. Electrical parameters like dc resistivity and drift mobility were reported with function of temperature and dopant concentration from room temperature to well beyond Curie temperature and explained with hopping mechanism between $\text{Fe}^{2+} \leftrightarrow \text{Fe}^{3+}$ ions. The activation energies in ferri and para magnetic regions were investigated. Dielectric parameters like dielectric constant, dielectric loss and ac conductivity were investigated variation with frequency and composition.

Keywords: nano-ceramics, citrate-gel auto combustion technique, structural parameters, magnetic properties, electrical properties, dielectric properties

1. Introduction

In the field of science and technology nanoscale ceramics are play an very important role because the nanostructure ceramic material are show evidence of novel properties and all other properties together are different than that of their bulk ceramic materials [1, 2]. From the past few years researchers are focus to result new materials used in cooling and energy conversion system [3]. Hence, nano-sized ceramic materials have the most important because nano-sized material structure, magnetic and electrical properties studies and their interrelation is still incomplete.

Among magnetic ceramic materials, spinal structure ceramics are most significant materials for research in fundamental electronic components due to their tremendous magnetic and electrical properties [4, 5]. The spinal structure ceramics are quite stable and they are important in a wide range of technological applications like magnetic recording, sensors, magnetic resonance imaging, transformer etc. [6, 7]. These materials are used as high frequency magnetic materials, microwave

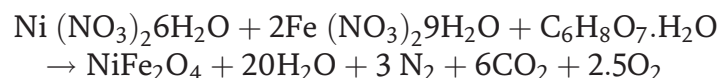
applications and data storage devices due to its high electrical resistivity values [8]. Nano-sized spinel ceramics are important dielectric materials in high frequency applications due to their high resistivity, low magnetic and dielectric losses [9, 10]. These materials are possess with high dielectric constant at low frequencies (10^2 - 10^5 Hz) with low conductivity. Hence these are use in microwave applications and several devices like high frequency transformer cores, resonators, switches and phase shifter etc. [11, 12].

Presently, many researchers are focused on preparation the nanoscale dimension ceramics because they have incredible changes in their properties, therefore these ceramics are largely synthesized in nanoscale for new and improved properties such as low saturation magnetization, enhanced coercivity etc. [13, 14]. Since last few years, numbers of wet chemical methods are developed to synthesis nano-sized spinel ceramic materials and these methods advantage over the physical methods to prepare homogeneity materials. Several chemical methods are used to prepare the material samples like electro-deposition [15], co-precipitation [16], micro emulsion method [17], glyoxylate precursor technique [18], hydrothermal technique [19], reverse micelle method [20], Solid state reaction [21], Sol-gel method [22] and Citrate-gel technique [23]. In most recent research work, Citrate-gel auto combustion technique attained immense significance, since it provides the pure and homogeneous nanoparticles and cost is low as compared to other chemical processes [24].

Among the spinel ceramics, Ni nano ceramic is a soft ferrimagnetic material due to its nanocrystalline nature and it useful for novel applications like gas sensing [25] and drug delivery [26]. In the recent years nano-sized Ni ceramic and substituted Ni nano ceramic extensively studied due to having high electrical resistance, low cost, high mechanical hardness, and eddy current losses low etc. [27, 28]. These material scientifically interest because of its promising and interesting applications in microwave devices, color imaging, magnetic refrigerators and high density recording devices [29]. Particularly trivalent like Cr is substituted in it, it's fascinating effect on electromagnetic and dielectric properties of nickel nano ceramics. From a review of earlier work it is evident that very less attention has been paid to study of structural, magnetic, electrical and dielectric properties in systematic manner.

2. Experimental technique

Nano ceramics chemical composition $\text{NiCr}_x\text{Fe}_{2-x}\text{O}_4$ ($x = 0.1, 0.3, 0.5, 0.7, 0.9$ and 1.0) have been prepared with Nickel nitrate, Chromium nitrate, Ferric nitrate, Citric acid and Ammonia as raw materials at low temperature by citrate-gel auto combustion technique.



Calculated quantities of the molar quantity AR grade of metal nitrates described in the starting materials by sensitive digital balance and they were dissolved in deionized double distilled water in separate in 100 ml beakers. The metal nitrates solutions are mixed together in beaker and added the citric acid in 1:3 ration of nitrate to citric acid; it was systematically stirred placed on magnetic hot plate stirrer. To this nitrate-citrate mixture added the ammonia to maintain the p^{H} to 7. The homogeneous solution was heated at about 80°C and to attain a thick gel. Further heated the gel maintained at a temperature of 180 – 200°C . Finally, water molecules were removed from the mixture, the viscous gel then began frothing.

The gel starts auto combustion reaction with flameless express in the most up-to-date regions of the beaker and it spread from the bottom to the top, the reaction was finished in a couple of minutes produced the structure with branched tree in an dark gray loose-fitting product. Finally the as-burnt ferrite powders were grained by using Agate Mortar and Pestle then calcined in programmable furnace through “Eurotherm” programmer-cum-controller at 700°C for 5 hr. The calcined ferrite powders were again grained by using Agate Mortar and Pestle to obtain a better crystallization and homogeneous distribution in the spinel. The step by step procedure for the synthesis of Nano ceramics is shown in the form of flow chart in **Figure 1**. For electrical and dielectric measurement pellet was prepared with KBr hydraulic press (Model: M-15) in 2–3 mm thickness and 10 mm diameter size.

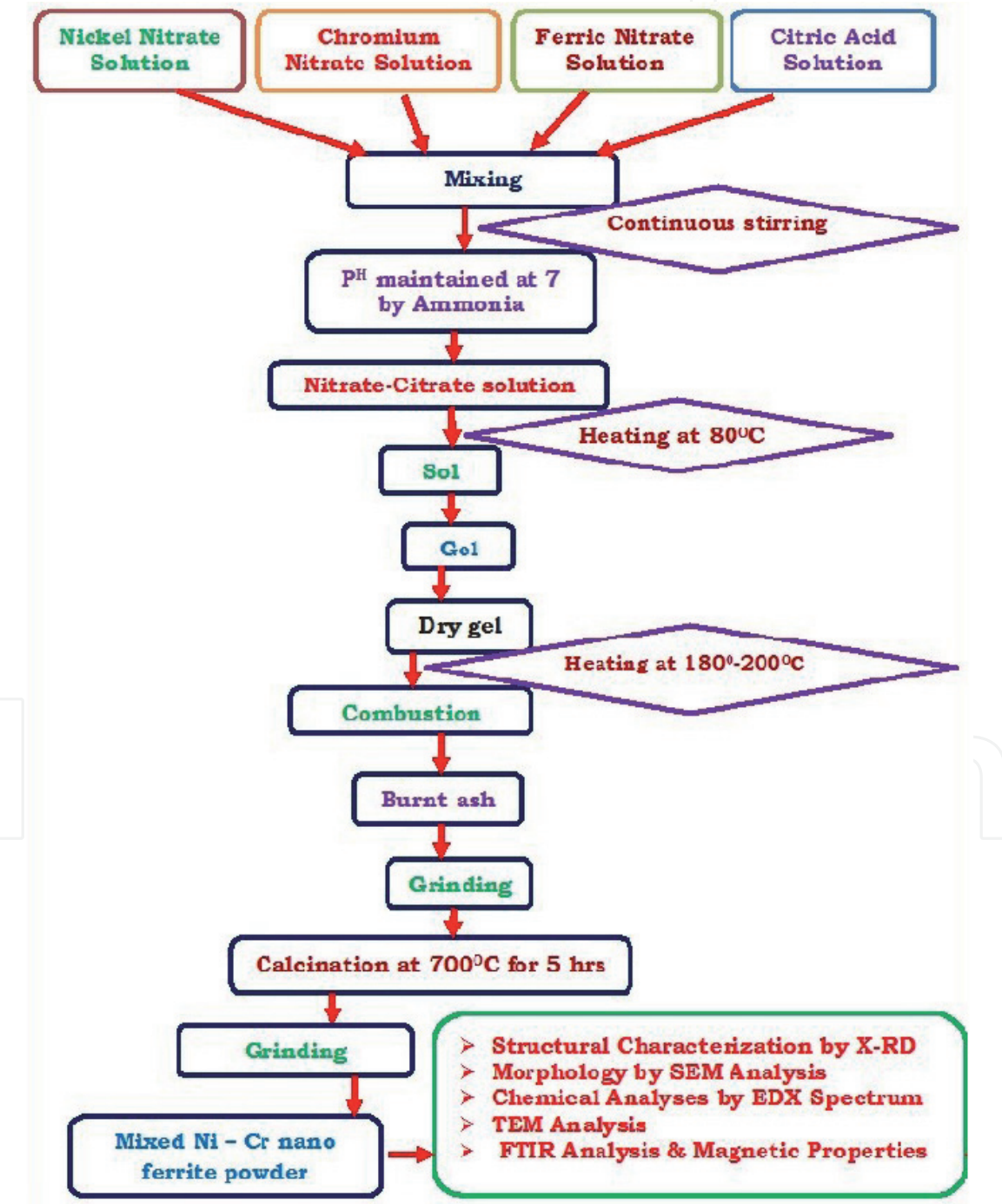


Figure 1.
Flow chart for the synthesis of Ni-Cr nano ferrites using Citrate-gel auto combustion technique.

The X-ray diffraction analysis was studied by Diffractometer Bruker (Karlsruhe, German) D8 advanced system with Cu K α radiation ($\lambda = 1.5405\text{\AA}$) between phase angle 20° to 80° by step $0.04^\circ/\text{sec}$ and scanning speed of 1.5 sec/step .

The prepared samples crystallite sizes were measured using the Scherer's Equation [30]

$$D_{hkl} = \frac{0.91 \lambda}{\beta \cos \theta} \quad (1)$$

Where D_{hkl} is the crystalline size perpendicular to (h k l) plane, λ is the incident X-ray wave length, β is the full width half maxima (FWHM) of (311) peak, and θ is the peak position (Bragg's angle at (311) peak).

The lattice parameter value is measured with the following equation:

$$a = \frac{d_{hkl}}{\sqrt{h^2 + k^2 + l^2}} \quad (2)$$

Hopping length at Tetrahedral (A-site) and Octahedral (B-site) were measured by following relations.

$$\text{A site (Tetrahedral) hopping length } d_A = 0.25a\sqrt{3} \quad (3)$$

$$\text{B site (Octahedral) hopping length } d_B = 0.25a\sqrt{2} \quad (4)$$

The X-ray density (d_x) measured with the following relation:

$$d_x = \frac{8M}{Na^3} \left(\frac{g}{cm^3} \right) \quad (5)$$

Where 8 is the number of molecules in a unit cell, M is the composition molecular weight, and N is the Avogadro's number.

The bulk density d_m was determined using formula:

$$d_m = \frac{m}{\pi r^2 h} \quad (6)$$

Where m is the sample mass, r is the sample radius, and h is the sample thickness. The porosity (P) of the ferrite was determined using formula:

$$P = 1 - \frac{d_m}{d_x} \quad (7)$$

Where d_m is the bulk density and d_x is the X-ray density.

The surface morphology was performed by using SEM technique (Scanning Electron Microscope). Elemental analysis was analyzed by energy dispersive X-ray spectroscopy (EDS). The calcined powders microstructure and average crystallite size were characterized by TEM (Tecnai-12, FEI, Netherlands) technique. FTIR gives the absorption band positions and it analyzed to get structural information about the prepared ferrite systems.

The magnetic properties were carryout at room temperature with obtained M-H loops by using VSM (GMW Magnet System, model 3473) From M-H loops saturation magnetization (M_s) and coercivity (H_c) are directly extracted. From the above measurements calculated the following parameters.

The anisotropy constant (K) was calculated with the following relation [31]:

$$H_c = \frac{0.98K}{M_s} \quad (8)$$

The magnetic moment (μ_B) was calculated with the following relation [32]:

$$\mu_B = \frac{M_w X M_s}{5585} \quad (9)$$

Where M_w is the composition molecular weight, M_s is the saturation magnetization. The Yefet-Kittel (Y-K) angles are calculated with the following relation [33]:

$$\mu_B = (6 + x) \cos \alpha_{Y-K} - 5(1 - x) \quad (10)$$

Where x is the Cr^{3+} concentration.

Temperature and composition dependent dc electrical properties were measured with two probe method [34].

The resistivity (ρ) and temperature (T) Kelvin relationship may be expressed as Arrhenius relation [35].

$$\rho = \rho_o e^{\Delta E / K_B T} \quad (11)$$

Where ρ_o is the resistivity at room temperature, K_B is the Boltzmann constant ($8.617 \times 10^{-5} \text{ eV K}^{-1}$), and ΔE is the activation energy;

The activation energies were measured with the following relation:

$$\Delta E = 2.303 X K_B X 10^3 X \text{slope} \text{ (eV)} \quad (12)$$

The drift mobility (μ_d) of charge carriers were measured with the following relation [36].

$$\mu_d = \frac{1}{\eta e \rho} \quad (13)$$

Where η is the number of charge carriers, e is the electron charge, and ρ is the resistivity at a given temperature.

The charge carrier concentration measured with the following relation [37]:

$$\eta = \frac{N_A d_B P_{Fe}}{M} \quad (14)$$

Where M is the sample molecular weight, N_A is the Avogadro number, d_B is the bulk density, and P_{Fe} is the number of iron atoms in ferrite composition.

Dielectric properties of the prepared pellets measured in between 20 to 2 MHz frequency at room temperature with LCR meter. Dielectric properties like dielectric constant loss tangent and ac conductivity were determined by the following formulae.

The dielectric constant was measured with the following relation [38]:***

$$\epsilon' = \frac{Cd}{\epsilon_o A} \quad (15)$$

Where C is the material capacitance, ϵ_o is the permittivity of the air ($8.854 \times 10^{-12} \text{ Fm}^{-1}$)

The AC conductivity was measured with the following relation [39]:

$$\sigma_{ac} = \omega \epsilon_0 \epsilon' \tan \delta \tag{16}$$

Where ϵ_0 is the permittivity of free space ($8.854 \times 10^{-12} \text{F/m}$), ϵ' is the dielectric constant, and $\tan \delta$ is the loss tangent.

3. Results and discussion

3.1 Structural characterization

3.1.1 XRD analysis

X-ray diffraction pattern of Ni-Cr nano ceramic particles is depicted in **Figure 2**. It shows the crystalline phases were identified with standard data PDF# 862267 from the ICDD data. It was observed that X-ray diffraction pattern can be well indexed with peaks corresponding to cubic spinel structure such as (111), (220), (311), (400), (511), (440), and (533). The highest reflection comes from (311) peak that shows spinel structure and all samples represents formation of cubic spinel structure in single phase without other evident additional impurity phases or secondary phases for chromium substituted nickel nano ceramic [40]. The crystallite size was computed and is given in **Table 1**. It shows that the prepared samples crystallite size is in the nanometer scale between 8.55 nm–10.36 nm.

Figure 3 shows the slightly decreases the lattice parameter with dopent Cr ion increases in mixed Ni-Cr ceramics, that means it obeys Vegard’s law [41]. It is because of the large ionic radii of Fe^{3+} (0.67\AA) is replaced by low ionic radius Cr^{3+} (0.64\AA) in B site [42]. Similar behavior was reported in Ni-Cr nanoceramic system [43].

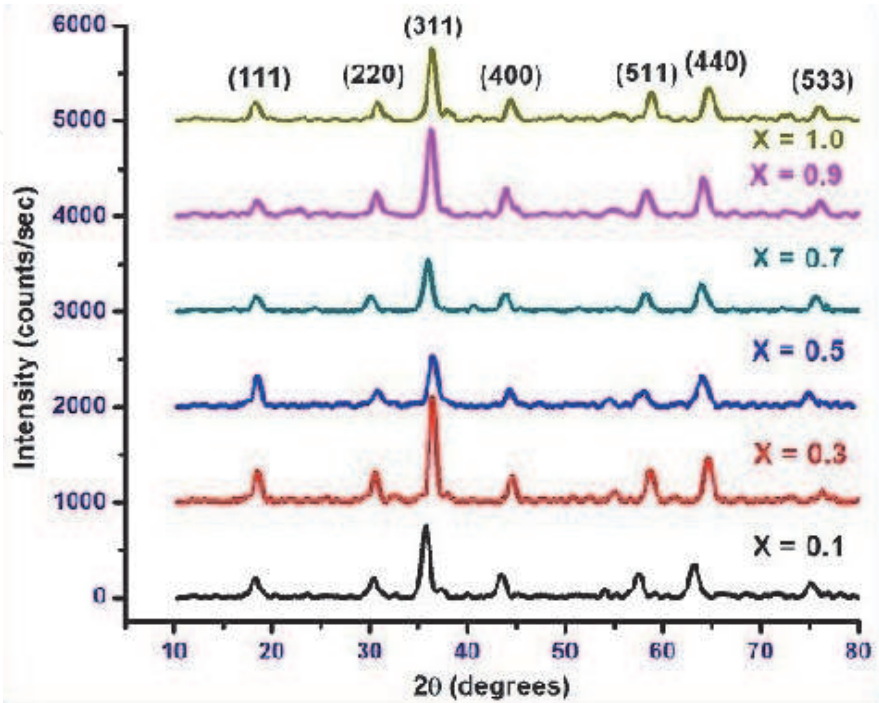


Figure 2.
X-ray diffraction pattren of mixed $\text{NiCr}_x\text{Fe}_{2-x}\text{O}_4$ nano ferrites.

Sl. No.	Composition	Crystallite size (nm)	Lattice parameter (a) (Å)	Hopping length		X-ray density (gram/cc)	Bulk Density (gram/cc)	Porosity (P %)
				(A-site) (d _A) (Å)	(B-site) (d _B) (Å)			
1	NiCr _{0.1} Fe _{1.9} O ₄	8.96	8.356	3.618	2.954	5.326	5.218	2.01937
2	NiCr _{0.3} Fe _{1.7} O ₄	10.36	8.342	3.612	2.949	5.334	5.192	2.67538
3	NiCr _{0.5} Fe _{1.5} O ₄	7.95	8.329	3.606	2.944	5.34	5.07	5.0628
4	NiCr _{0.7} Fe _{1.3} O ₄	8.55	8.316	3.601	2.940	5.35	5.012	6.31649
5	NiCr _{0.9} Fe _{1.1} O ₄	8.84	8.301	3.594	2.934	5.36	4.941	7.82673
6	NiCrFeO ₄	9.26	8.293	3.591	2.932	5.368	4.813	10.3369

Table 1.
Structural analysis of synthesized and heat treated NiCr_xFe_{2-x}O₄ nano ferrites.

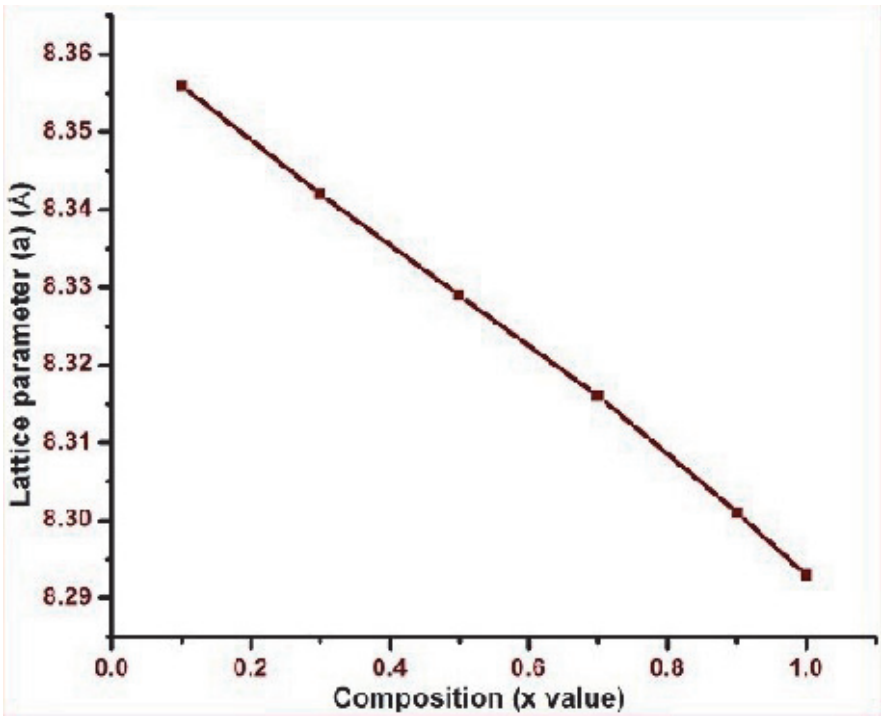


Figure 3.
Lattice parameter variation with Cr concentration.

The measured hopping lengths are given in **Table 1**. It shows the decreases the distance between magnetic ions with increase Cr ion concentration in Ni nano ceramic, which makes decreasing the hopping length. It may be due to that Cr³⁺ ion (0.63Å) has smaller radius than Fe³⁺ ion (0.67Å). Similar trend was studied for the Ni-Cr ceramic system prepared by impregnation technique [44].

The density measurements were illustrated in **Table 1**. It was found that **Figure 4** shows the increases of the X-ray density (dx) from 5.326 to 5.368 gram/cc and the bulk density (dm) decreases from 5.218 to 4.813 gram/cc with increases Cr³⁺ ions concentration in nickel nanoferrite. It may be because of larger atomic weight and density of Fe (55.847gm/mole, 7.874gm/cm³) compare with atomic weight and density of Cr (51.996gm/mole, 7.14gm/cm³). The X-ray density is more than the apparent density due to the existence of pores which depends on the preparation state. Porosity increase with increase Cr ion concentration and it shows similar behavior of X-ray density. Similar behavior observed for the Cr substitution nano ceramic system with other researcher reports [45, 46].

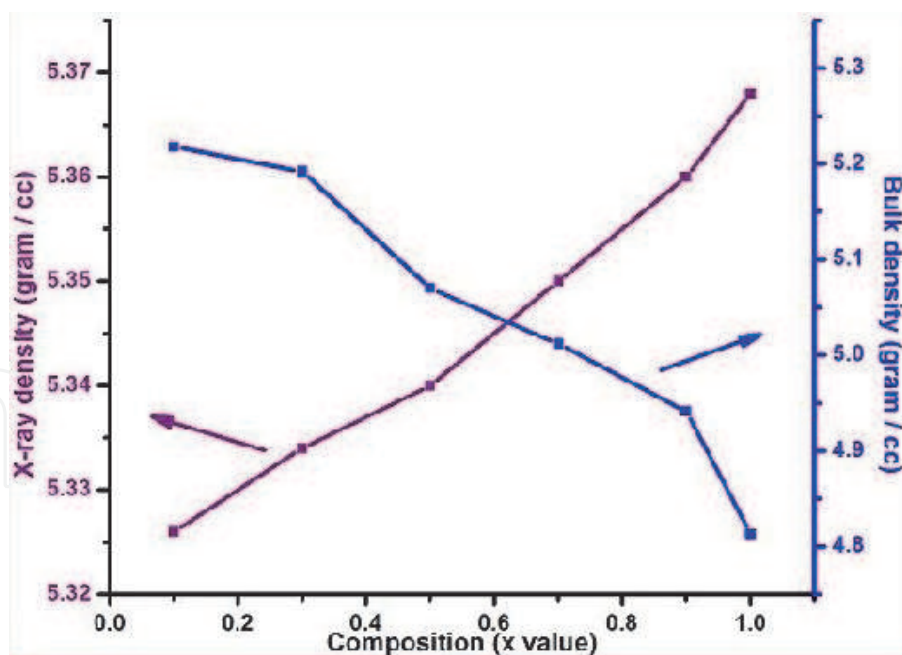


Figure 4.
X-ray density and bulk density variation with Cr concentration.

3.1.2 Morphological studies

The SEM representative micrographs of the prepared Ni-Cr nanoceramic system, with various Cr concentration, are shown in **Figure 5(a-f)**. It shows that the morphology is similar and they are in nanoscale with almost inhomogeneous. The obtained patterns energy dispersive X-ray spectroscopy of various composition of Ni-Cr nanoceramic systems are shown in **Figure 5(a-f)**. The corresponding elemental and atomic percentage of various chromium concentrations were illustrated in **Table 2**. It reveals that the compositions representing the elements Ni, Cr, Fe, and O without precipitating cations

TEM micrographs of $\text{NiCr}_{0.3}\text{Fe}_{1.7}\text{O}_4$ and $\text{NiCr}_{0.7}\text{Fe}_{1.3}\text{O}_4$ nanoceramics are represented in **Figure 6(a)** and **6(b)**. The crystallite size is in nanometer scale and also be in agreement well with crystallite size estimated from XRD analysis.

3.1.3 FTIR analysis

The FTIR spectra of the mixed $\text{NiCr}_x\text{Fe}_{2-x}\text{O}_4$ nanoceramic, recorded in the range of $400\text{--}4000\text{ cm}^{-1}$, is shown in **Figure 7** and absorption band results are reported in **Table 3**. It shows the two absorption bands ν_1 and ν_2 at around 600 cm^{-1} and 400 cm^{-1} respectively. The high frequency band (ν_1) corresponds to $\text{Fe}^{3+}\text{-O}^{2-}$ vibrations at tetrahedral (A site) and low frequency band (ν_2) corresponds to $\text{M}^{+2}\text{-O}^{2-}$ vibrations at octahedral sites (B site) [47] and these are representing the spinel ceramic in single phase [48]. The bands around 3400 cm^{-1} , 2400 cm^{-1} and 1600 cm^{-1} are the contribution of the stretching vibration of free and absorbed water, indicated the removal of the -OH, -CO and -NO groups. Similar trend have been observed for Ni-Cr nano ceramic system prepared with impregnation technique by others [49, 50].

3.2 Magnetic properties

The obtained magnetic hysteresis loops are illustrated in **Figure 8**. It shows that the loop area is very narrow therefore the samples present soft ferrite nature with

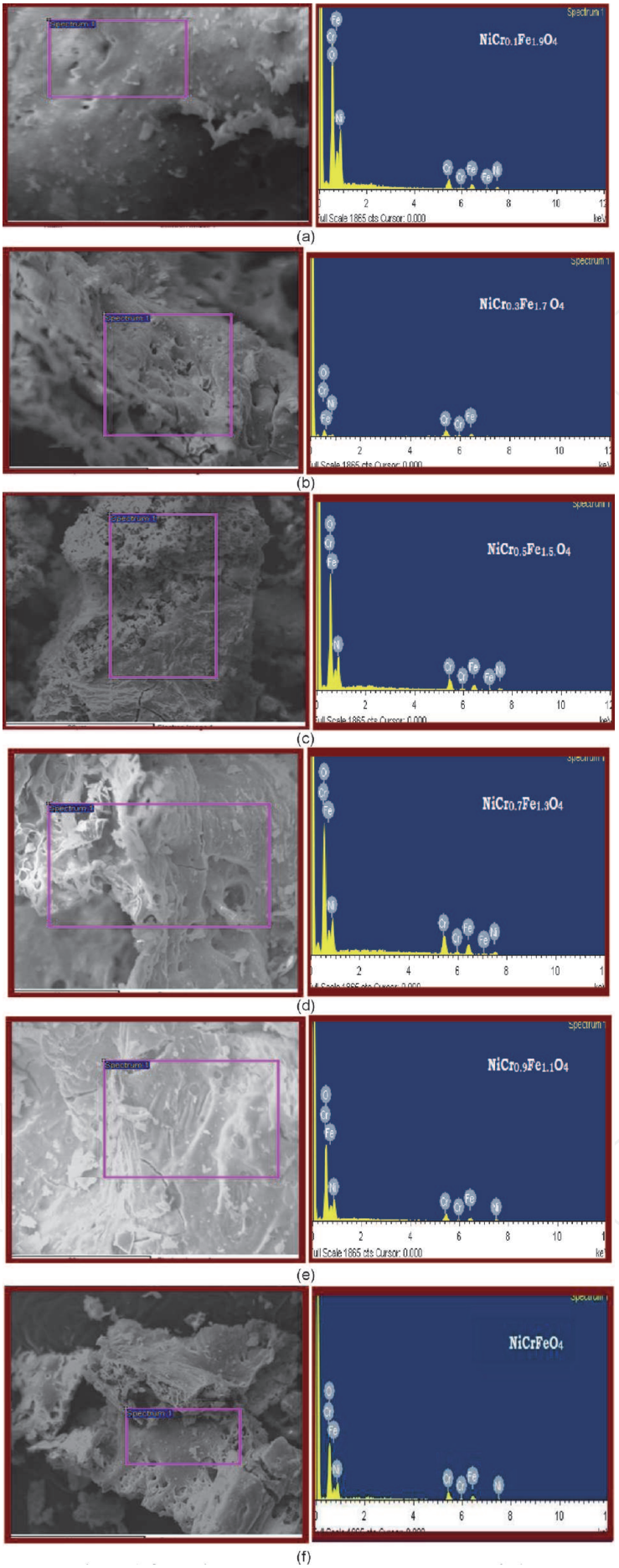


Figure 5.
(a-f) SEM images and EDS images of $\text{NiCr}_x\text{Fe}_{2-x}\text{O}_4$ nano ferrites. (a) $\text{NiCr}_{0.1}\text{Fe}_{1.9}\text{O}_4$ ($X = 0.1$), (b) $\text{NiCr}_{0.3}\text{Fe}_{1.7}\text{O}_4$ ($X = 0.3$), (c) $\text{NiCr}_{0.5}\text{Fe}_{1.5}\text{O}_4$ ($X = 0.5$), (d) $\text{NiCr}_{0.7}\text{Fe}_{1.3}\text{O}_4$ ($X = 0.7$), (e) $\text{NiCr}_{0.9}\text{Fe}_{1.1}\text{O}_4$ ($X = 0.9$), and (f) NiCrFeO_4 ($X = 1.0$).

Element	O		Fe		Ni		Cr	
Ferrite composition	Element %	Atomic %	Element %	Atomic %	Element %	Atomic %	Element %	Atomic %
NiCr _{0.1} Fe _{1.9} O ₄	17.01	41.45	29.07	21.80	27.72	19.35	26.20	17.40
NiCr _{0.3} Fe _{1.7} O ₄	19.50	45.20	29.47	21.99	25.02	16.67	26.01	16.14
NiCr _{0.5} Fe _{1.5} O ₄	19.16	44.87	33.03	23.81	24.28	16.30	23.53	15.02
NiCr _{0.7} Fe _{1.3} O ₄	19.79	45.86	30.76	21.96	27.30	18.14	22.15	14.04
NiCr _{0.9} Fe _{1.1} O ₄	17.55	42.24	31.56	24.11	27.89	19.23	23.00	14.42
NiCrFeO ₄	20.41	46.97	27.28	19.32	23.00	14.42	24.72	15.51

Table 2.
Elements of each sample composition analyzed by EDS pattern.

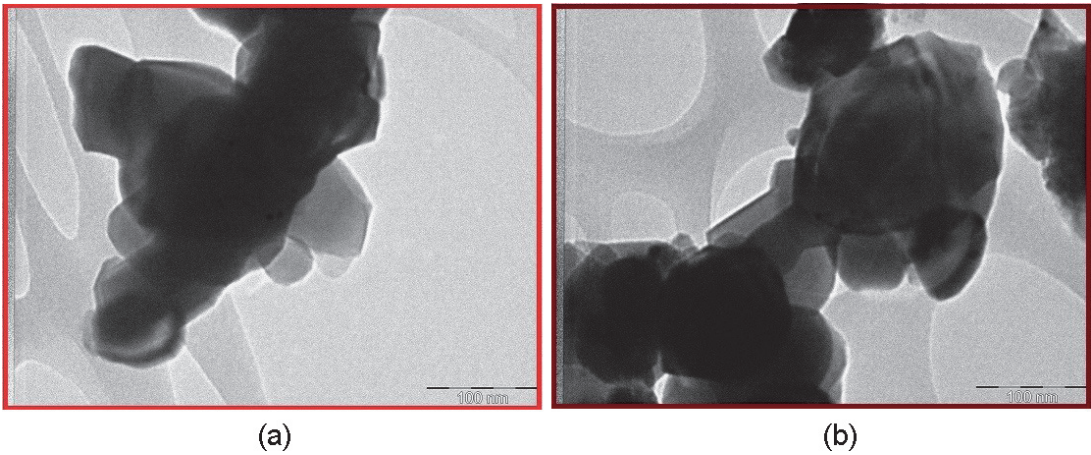


Figure 6.
(a) TEM image of NiCr_{0.3}Fe_{1.7}O₄ nano ferrite. (b) TEM images of NiCr_{0.7}Fe_{1.3}O₄ nano ferrite.

less coercivity [51]. The measured magnetic properties of Ni-Cr nano ceramics at room temperature were reported in **Table 4**.

It is observed that the Ni-Cr nanoceramics have less saturation magnetization and less coercivity due to the smaller grain size, as illustrated in **Table 4**. That means the grain size is small, the saturation magnetization is less. The saturation magnetization decreases from 4.49 to 2.97 emu/gr with increases of the Cr³⁺ concentrations in Ni nanoceramics at room temperature, as evident in **Figure 9**. Because of that less magnetic moment Cr³⁺ ions (~3μ_B) are substituted in the place of higher magnetic moment Fe³⁺ ions (~5μ_B) at octahedral sublattice. As increases Cr³⁺ ion concentration, decreases the iron ions ratio between octahedral and tetrahedral sites. As a result, super exchange interaction between A-site & B-site decreases. Which lead to decrease in saturation magnetization. It is attributing to the weak magnetic interactions in Ni-Cr ceramics. Therefore, material becomes converted into soft magnetic material. Similar report was observed by Bhukal et al. [52].

The measured Coercitive field values are reported in **Table 4**. It shows that this parameter decreases from 136.19 to 63.03 Oe (minimum for x = 0.7 composition) and thereafter it increases to 106.08 Oe with increases the Cr³⁺ concentration in nickel nanoceramic. It shows that decreases in coercive field with increase Cr³⁺ ion concentration because of anisotropy field decreases which in order decreases the domain wall energy [53]. Increases in coercive field with composition X = 0.9 and 1.0 due to anisotropy field increases which in order domain wall energy increases [54, 55].

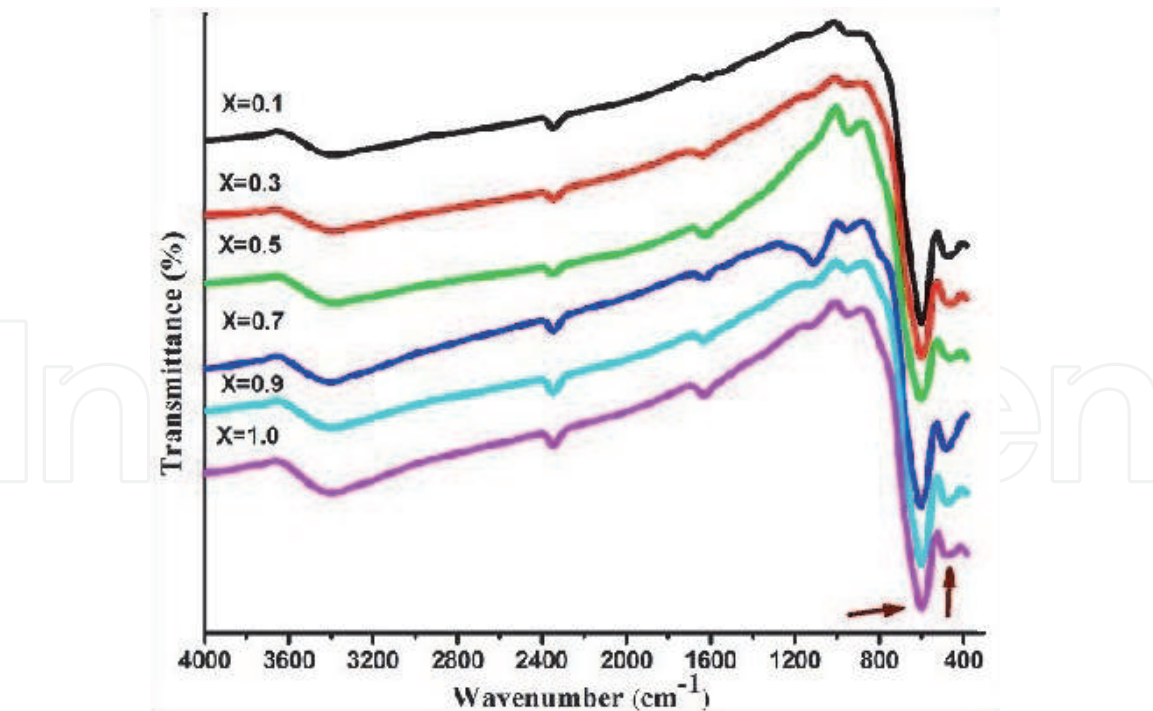


Figure 7.
FT-IR patterns of mixed $\text{NiCr}_x\text{Fe}_{2-x}\text{O}_4$ nano ferrites.

Sl.No.	Composition	$\nu_1 \text{ (cm}^{-1}\text{)}$	$\nu_2 \text{ (cm}^{-2}\text{)}$
1	$\text{NiCr}_{0.1}\text{Fe}_{1.9}\text{O}_4$	599.962	485.354
2	$\text{NiCr}_{0.3}\text{Fe}_{1.7}\text{O}_4$	607.036	477.055
3	$\text{NiCr}_{0.5}\text{Fe}_{1.5}\text{O}_4$	602.453	479.694
4	$\text{NiCr}_{0.7}\text{Fe}_{1.3}\text{O}_4$	591.435	481.109
5	$\text{NiCr}_{0.9}\text{Fe}_{1.1}\text{O}_4$	594.864	492.428
6	NiCrFeO_4	597.132	472.619

Table 3.
FT-IR parameters of mixed Ni-Cr nano ferrites.

From **Table 4**, it shows that the magnetic moment values are decreases from $0.188\mu_B$ to $0.122\mu_B$ with increases Cr^{3+} ion concentrations in Ni nano ceramic. The decrease in magnetic moment is credited to greater tenancy of Cr^{3+} at B sites. Therefore the materials are getting changed into soft ferrite materials.

Magnetic moment values are low due to the Cr^{3+} ions substituted in nickel nano ceramic. It is explained based on the non-collinear spin arrangement [56, 57]. The B–O–B coupling interactions at the B sublattice become stronger than that of A–O–B coupling between magnetic ions at the A and B sublattice due to the presence of a small canting of the B site moment with respect to the direction of the A site moment. The B–O–B coupling leads to the random existence of the small canted structure at the B site and forms triangular configuration in the ferrite system. As a result, the magnetic moments of the Fe ions at the B site are shifted from the collinear parallel to nonparallel arrangements. Therefore, the saturated magnetization is being decreased corresponding to the magnetic moment which is also decreased.

The decrease of magnetization has been proposed by Yafet and Kittel(Y–K) by triangular arrangement of spins [58]. The Y-K angles of Ni-Cr nano ceramic system are reported here in the **Table 4**. It is clear that increases the Y-K angles with

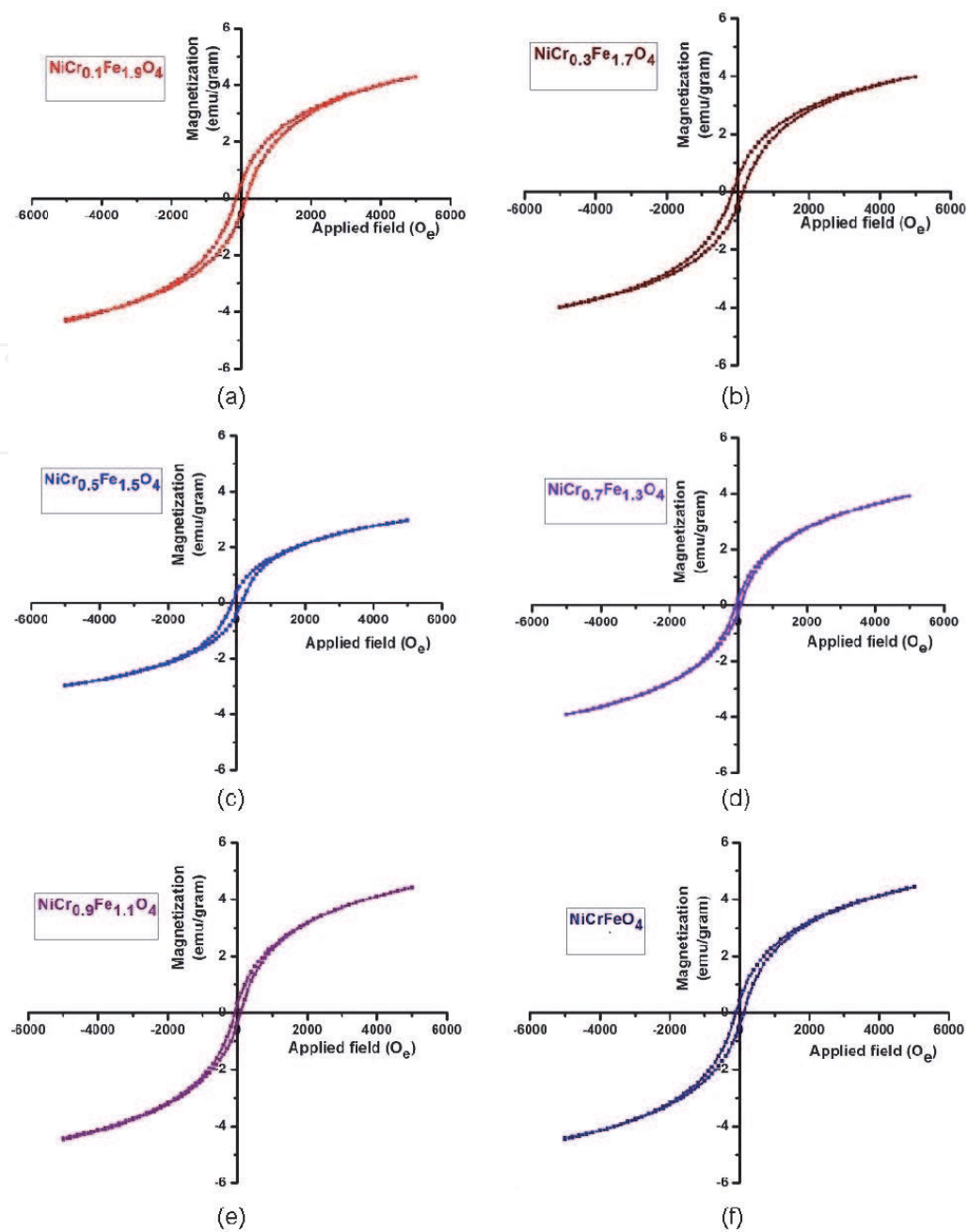


Figure 8. (a-f) Magnetic hysteresis loops for $\text{NiCr}_x\text{Fe}_{2-x}\text{O}_4$ nano ferrites. (a) $X = 0.1$, (b) $X = 0.3$, (c) $X = 0.5$, (d) $X = 0.7$, (e) $X = 0.9$, and (f) $X = 1.0$.

Sl. No.	Composition	Saturation magnetization (M_s)(emu/gr)	Coercive field (H_C) (O_e)	Magnetic moment (μ_B) (Bohr magneton)	Y-K angle (θ)
1	$\text{NiCr}_{0.1}\text{Fe}_{1.9}\text{O}_4$	4.49	136.19	0.18823	39.7751
2	$\text{NiCr}_{0.3}\text{Fe}_{1.7}\text{O}_4$	4.29	125.95	0.17911	54.2687
3	$\text{NiCr}_{0.5}\text{Fe}_{1.5}\text{O}_4$	4.15	116.58	0.17273	65.7204
4	$\text{NiCr}_{0.7}\text{Fe}_{1.3}\text{O}_4$	3.99	63.02	0.16529	75.6083
5	$\text{NiCr}_{0.9}\text{Fe}_{1.1}\text{O}_4$	3.67	79.19	0.15154	84.5817
6	NiCrFeO_4	2.97	106.07	0.12272	88.9955

Table 4. Magnetic parameters from hysteresis loops of mixed Ni-Cr nano ferrites.

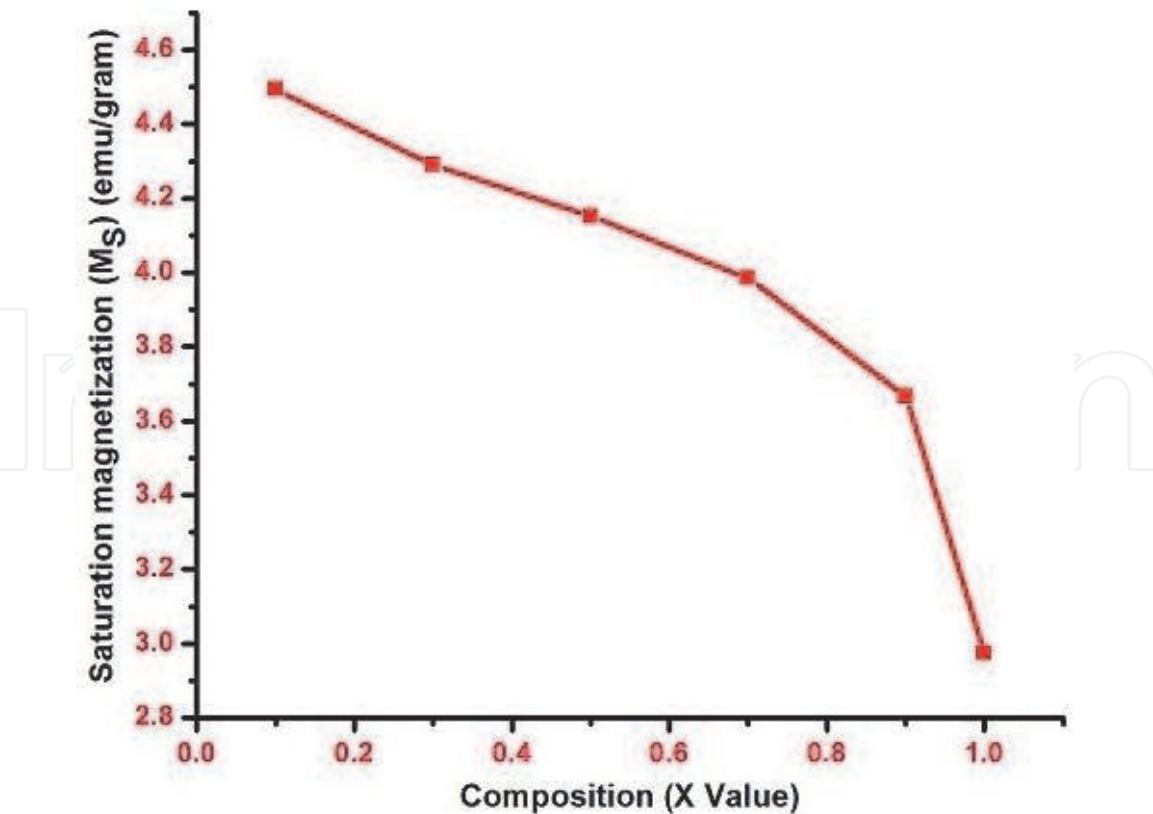


Figure 9.
Variation of saturation magnetization with Cr concentration.

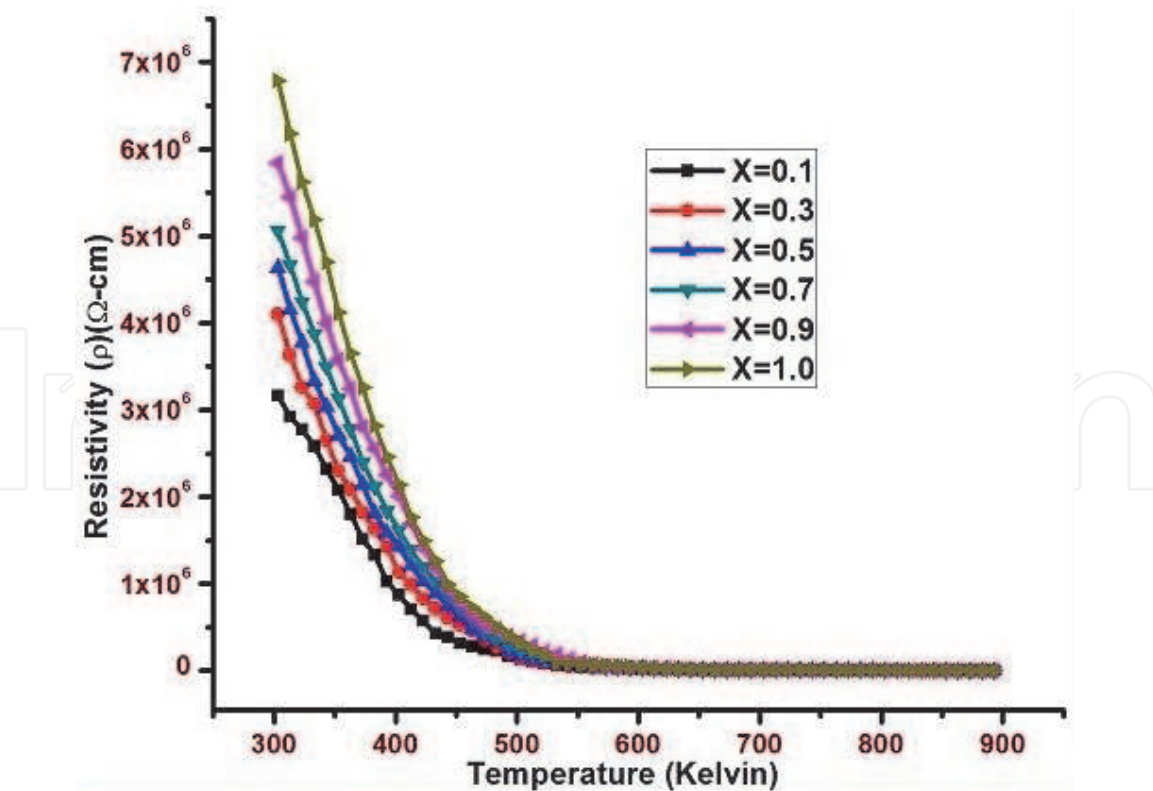


Figure 10.
DC resistivity variation with temperature of $\text{NiCr}_X\text{Fe}_{2-X}\text{O}_4$ nano ferrites.

increase Cr^{3+} ion concentration in Ni nano ferrite. It indicates that the spin canting takes place significantly at higher concentration of Cr content. Therefore, increases the spin arrangement at B-site. As a result, decrease A-B exchange interaction

consequent decreases in magnetization. From obtained hysteresis loops it is proved that the prepared samples are enhanced soft magnetic performance. Hence these materials are desirable for transformers and these are useful for low inductance cores and coils [59].

3.3 Electrical properties

DC resistivity variation with temperature of Ni-Cr nano ceramics are illustrated in **Figure 10**. It shows the normal behavior for semiconductors of prepared samples [60]. As temperature in increasing dc resistivity decreases because hopping rate is increases due to which activation of electrons jumps from Fe^{3+} to Fe^{2+} ions at B-sites. Similar trend reported by Iqbal et al. [61]. The calculated dc electrical values such as resistivity, conductivity, and drift mobility of Ni-Cr nano ceramic compositions at room temperature were reported in **Table 5**.

From **Table 5** the DC resistivity increases from $3.17.10^6$ to $6.79.10^6 \Omega\text{-cm}$ and the conductivity decreases from $3.15.10^{-7}$ to $1.47.10^{-7} \Omega\text{-cm}$, as given in **Figure 11**. It shows that the resistivity has increased and conductivity has decreased with Cr^{3+} ion concentration increase in Ni nano ceramic. Because of that Fe ($9.7 \times 10^{-6} \Omega\text{-cm}$) has smaller value of resistivity as compared with Cr ($1.3 \times 10^{-5} \Omega\text{-cm}$). Resistivity of Ni-Cr nano ferrites indicate that have high resistivity which show the way to low eddy current losses and they are popular in electronic inductors, transformers and electromagnets. Similar result was observed by Sagar E. Shirsath et al. [62].

Figure 12 shows the Arrhenius plots $\ln(\rho T)$ versus $10^3/T$ of Ni-Cr nano ceramic system, it observed that a change at a point, it indicates a change of magnetic ordering. The curve divided into two regions as ferrimagnetic region and paramagnetic region. Activation energy values of prepared samples are calculated and they are reported in **Table 6**. It shows that the activation energy values in paramagnetic region (E_p) are higher than those in ferrimagnetic region (E_f). Because of charge carriers need more energy for the conduction in paramagnetic region as compared with ferrimagnetic region. As a result, the conduction process is affected by the change in magnetic ordering. Similar results are reported by other researchers [63, 64].

It may be due to the replacement of Fe^{3+} ions with Cr^{3+} ions at B-sites [65]. Cr^{3+} ions are strongly preferred at octahedral site (B-site). When Cr ion substituted in Ni ceramic, Fe^{3+} ions are partially replaced with Cr^{3+} ions at octahedral site (B-site). Hence decrease the number of Fe^{3+}/Fe^{2+} ion pairs at octahedral site (B-site). Therefore decrease in hopping of ions consequently an increase in resistivity and decrease

Sl. No.	Composition	At room temperature			Curie temperature (T_C) (Kelvin)	
		DC Conductivity (σ) ($\Omega^{-1}\text{-cm}^{-1}$)	Resistivity (ρ) ($\Omega\text{-cm}$)	Drift mobility (μ_d) (cm^2/Vs)	DC Resistivity	Loria-Sinha technique
1	$NiCr_{0.1}Fe_{1.9}O_4$	3.15×10^{-07}	3.17×10^{06}	7.73×10^{-11}	775.39	789
2	$NiCr_{0.3}Fe_{1.7}O_4$	2.44×10^{-07}	4.10×10^{06}	7.55×10^{-11}	747.58	762
3	$NiCr_{0.5}Fe_{1.5}O_4$	2.16×10^{-07}	4.64×10^{06}	7.42×10^{-11}	705.32	729
4	$NiCr_{0.7}Fe_{1.3}O_4$	1.98×10^{-07}	5.06×10^{06}	7.29×10^{-11}	690.71	697
5	$NiCr_{0.9}Fe_{1.1}O_4$	1.71×10^{-07}	5.84×10^{06}	6.84×10^{-11}	659.53	678
6	$NiCrFeO_4$	1.47×10^{-07}	6.79×10^{06}	6.69×10^{-11}	635.34	642

Table 5.
DC electrical values of mixed Ni-Cr nano ferrites.

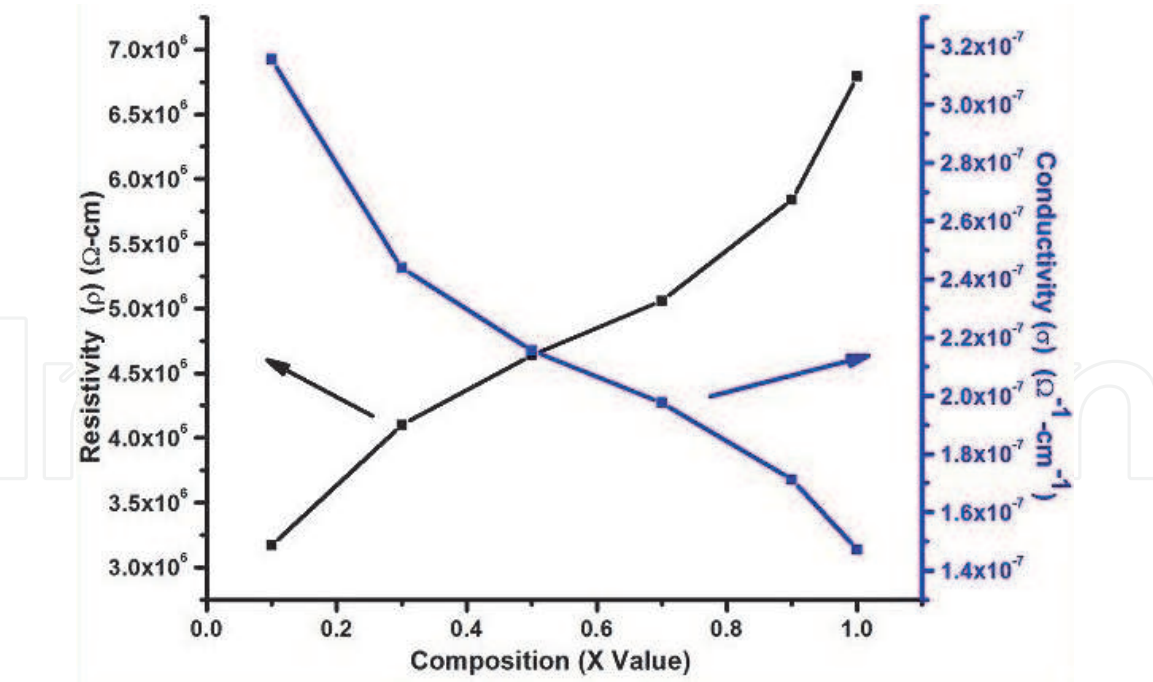


Figure 11.
DC resistivity and conductivity variation with Cr^{3+} concentration at room temperature.

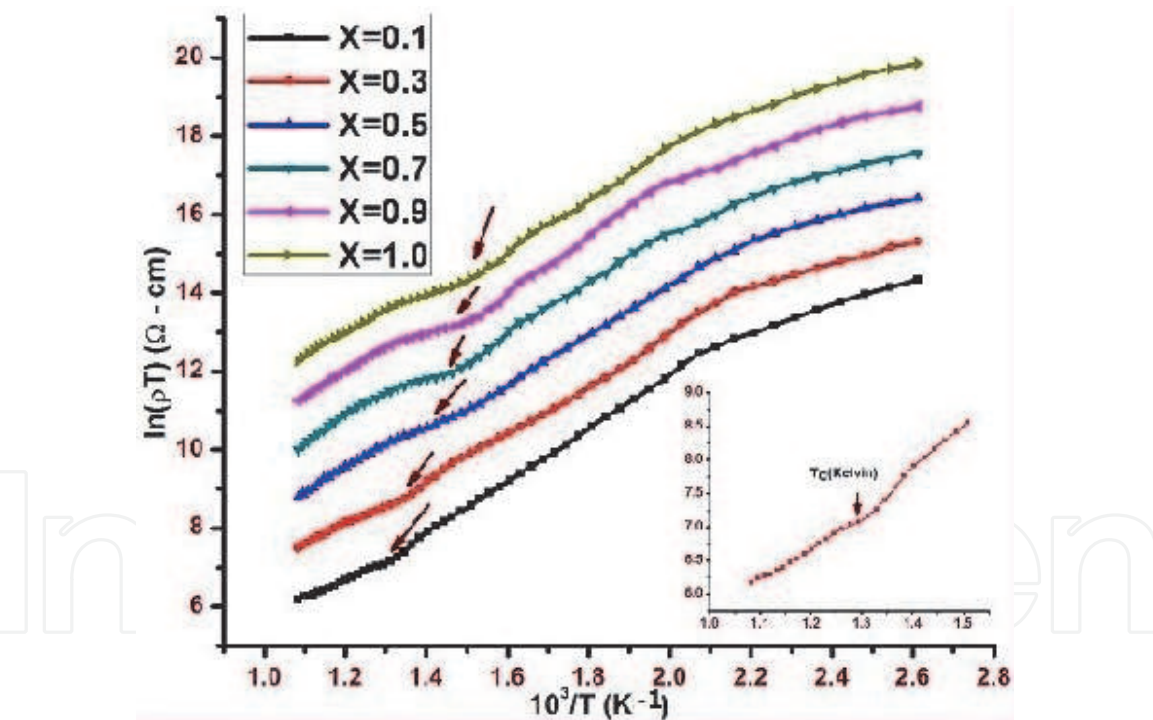


Figure 12.
DC resistivity variation with inverse temperature of $\text{NiCr}_x\text{Fe}_{2-x}\text{O}_4$ nano ferrites.

in conductivity with increases Cr^{3+} ion in Ni nano ceramic system. A similar behavior was reported by Khan et al. [66]. Hence, the activation energy increases from 0.167 to 0.341 eV with increase Cr^{3+} ions concentration in Ni nanoceramic systems (see **Figure 13**). Due to resistivity increases with increase in Cr^{3+} ion concentration. Similar result reported by others [67, 68].

The activation energy increases with increase in Cr^{3+} content (x) recommend that the Cr^{3+} ions are toward the inside into octahedral sites barricade the electron hopping between $\text{Fe}^{2+} \leftrightarrow \text{Fe}^{3+}$ ions for electrical conduction. This show the way to an

Sl.No.	Composition	Para region (E_p) ev	Ferri region (E_f) ev	Activation energy (ΔE) ev
1	NiCr _{0.1} Fe _{1.9} O ₄	0.412	0.244	0.167
2	NiCr _{0.3} Fe _{1.7} O ₄	0.522	0.324	0.197
3	NiCr _{0.5} Fe _{1.5} O ₄	0.635	0.394	0.241
4	NiCr _{0.7} Fe _{1.3} O ₄	0.726	0.44	0.286
5	NiCr _{0.9} Fe _{1.1} O ₄	0.794	0.489	0.305
6	NiCrFeO ₄	0.852	0.511	0.341

Table 6.
Activation energy values of mixed Ni-Cr nano ferrites.

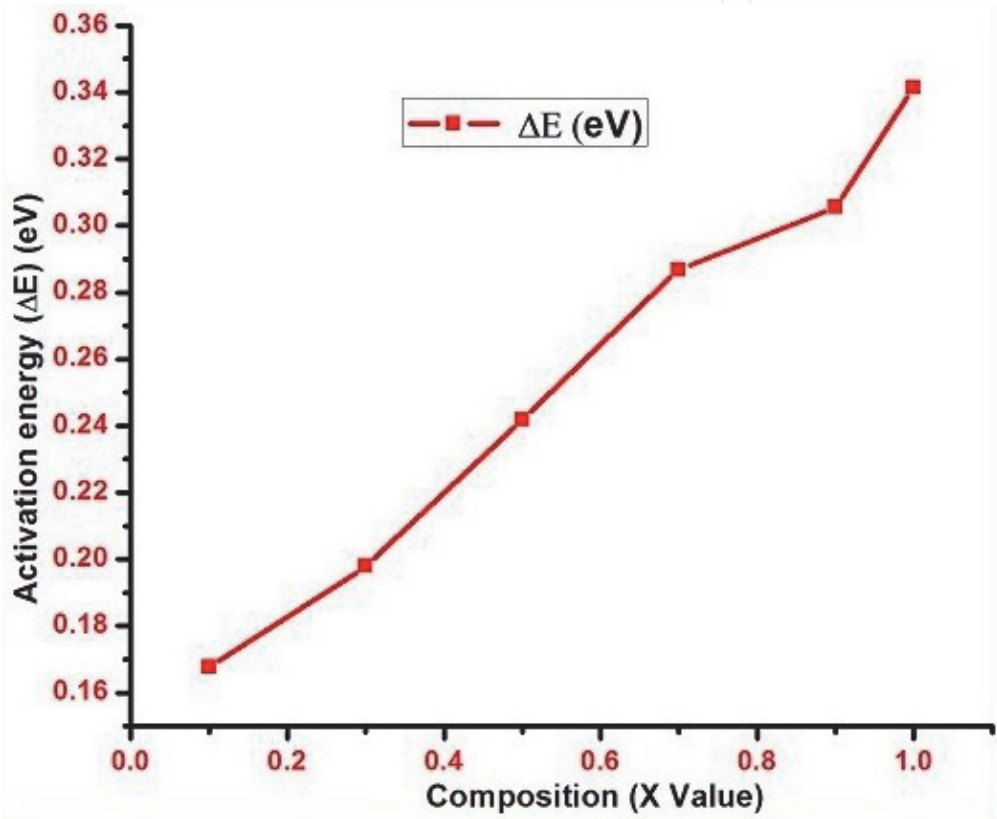


Figure 13.
Activation energy (ΔE) variation with Cr^{3+} concentration.

decrease in the conduction loss and increase in resistivity, as a result material with higher resistivity has higher values of activation energies and vice versa [69].

The drift mobility variation with temperature of Ni-Cr nano ceramic system reported in **Figure 14**. It shows that drift mobility increases with increase in temperature. Because the change in charge carrier mobility rather than the change in carrier concentration. Hence, that charge carriers begin hopping from one site to another site as increasing the temperature, therefore drift mobility increases. Similar result was observed by Bhukal et al. [70].

From **Table 5**, it shows that the drift mobility decreases from $7.73 \times 10^{-11} \text{ cm}^2/\text{Vs}$ to $6.69 \times 10^{-11} \text{ cm}^2/\text{Vs}$ with increases Cr^{3+} concentration in Ni nano ceramics. It is due to the material with higher resistivity have lower mobility and vice versa. The decreasing trend in drift mobility with the composition shown materials is good choice for high frequency applications. Similar results were also reported by Ashiq et al. [71].

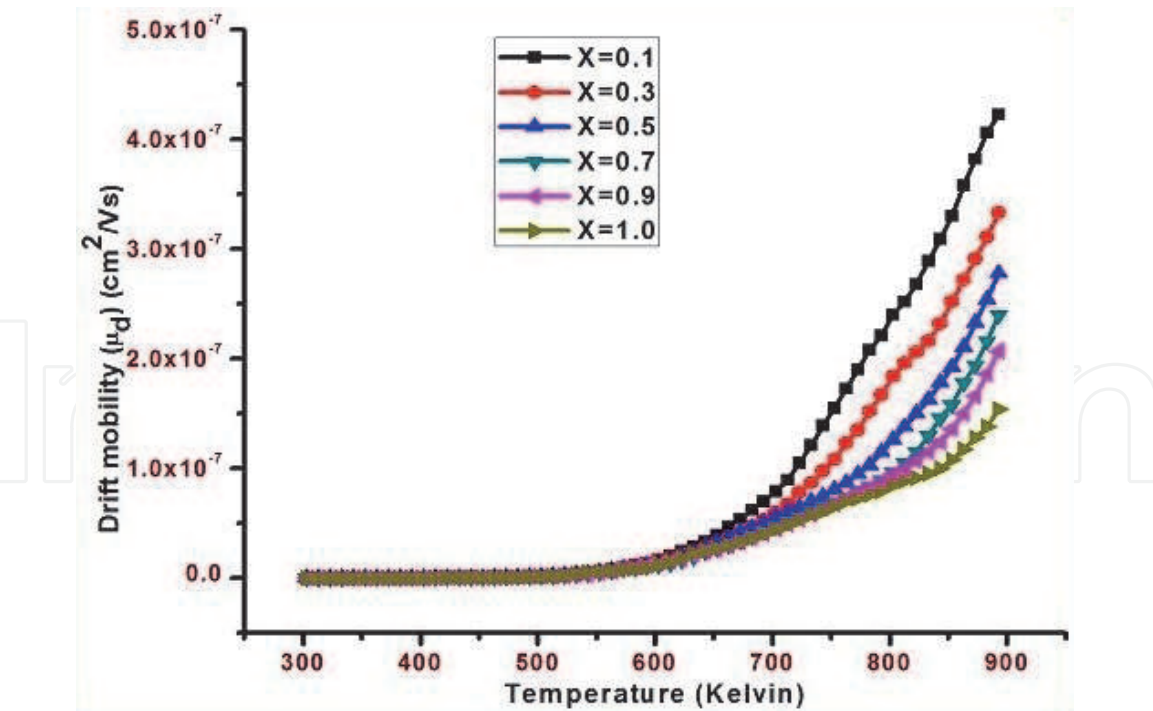


Figure 14.
Drift mobility variation with inverse temperature of $\text{NiCr}_X\text{Fe}_{2-X}\text{O}_4$ nano ferrites.

From Arrhenius plot of $\ln(\rho T)$ with $10^3/T$ as shown in **Figure 12**, straight line must take place a change at a particular temperature, there the ferrimagnetism will change into paramagnetism is known as Curie temperature. From dc resistivity measurements values of the Curie temperature with composition of the prepared samples and it has been determined by using another method (Loria-Sinha technique). The values were tabulated in **Table 5** as evident in **Figure 15**.

In the present study, from Loria-Sinha method, the Curie temperature is observed as decreases from 789 to 642 K and from DC resistivity experimental observation it was found to decreases from 775.39 to 635.34 K on increasing the Cr^{3+} ions concentration in Ni nanoceramics, due to the Fe^{3+} ions, which have been placed by paramagnetic Cr^{3+} ion concentration [72].

When the Fe^{3+} ion replacement with Cr^{3+} ion concentration increases, the magnetization decreases in B-sublattice without disturbing the A-sublattice, therefore decrease in A-B interaction hence, decreases in Curie temperature. Similar behavior was observed in the trivalent substitution nanoceramic system [73]. The Curie temperature results from Loria-Sinha method (gravity method) were good in agreement with determined transition temperature values by dc resistivity measurements.

3.4 Dielectric properties

The frequency dependence dielectric constant (ϵ') of Ni-Cr nano ceramic system represent in **Figure 16**. It is observed that at lower frequency dielectric constant is high and it decreases sharply and then decreases slowly with the increase in frequency and shows almost frequency independent behavior at high frequency range [74]. The variation of dielectric constant with frequency is explained according to Maxwell-Wagner theory [75, 76], which is in good agreement with Koop's phenomenological theory [77]. Similar kind of trend for dielectric constant with frequency was observed by others [78, 79].

The dielectric loss tangent ($\tan \delta$) variation with frequency is representing in **Figure 17**. It depicts the value of $\tan \delta$ increases initially and exhibits the loss factor,

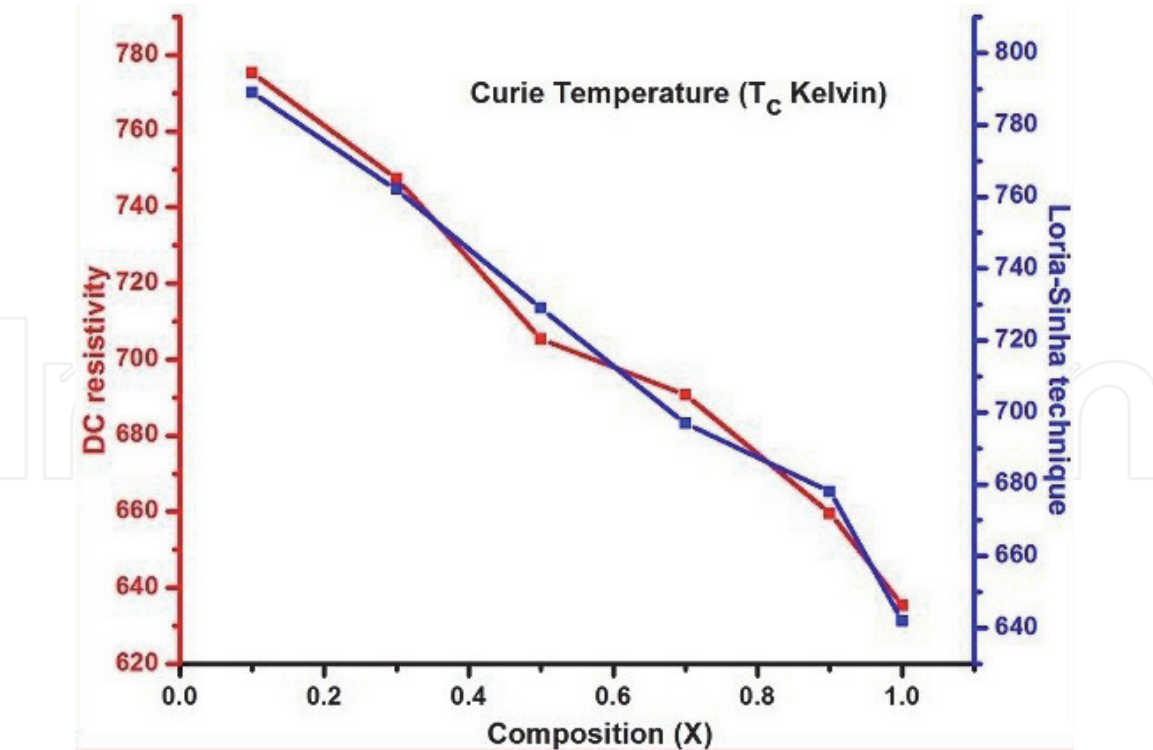


Figure 15.
Curie temperature variation with Cr^{3+} concentration.

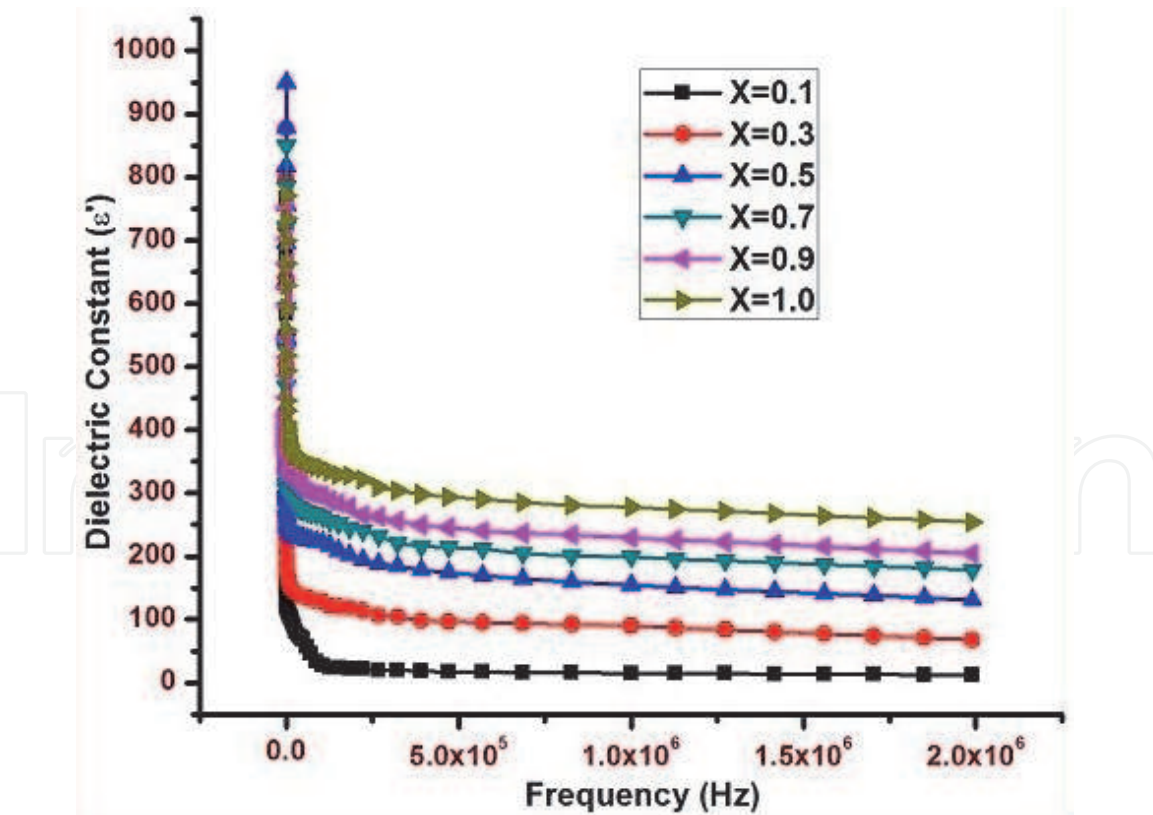


Figure 16.
Dielectric constant (ϵ') variation of Ni-Cr nano ferrites with frequency.

which is maximum between 1.103 to 4.104 Hz, and further decreases by increasing the frequency. It shows the Debye-type relaxation and this type of peaking behavior is observed when the jumping frequency between $\text{Fe}^{2+} \leftrightarrow \text{Fe}^{3+}$ ions is exactly equal to

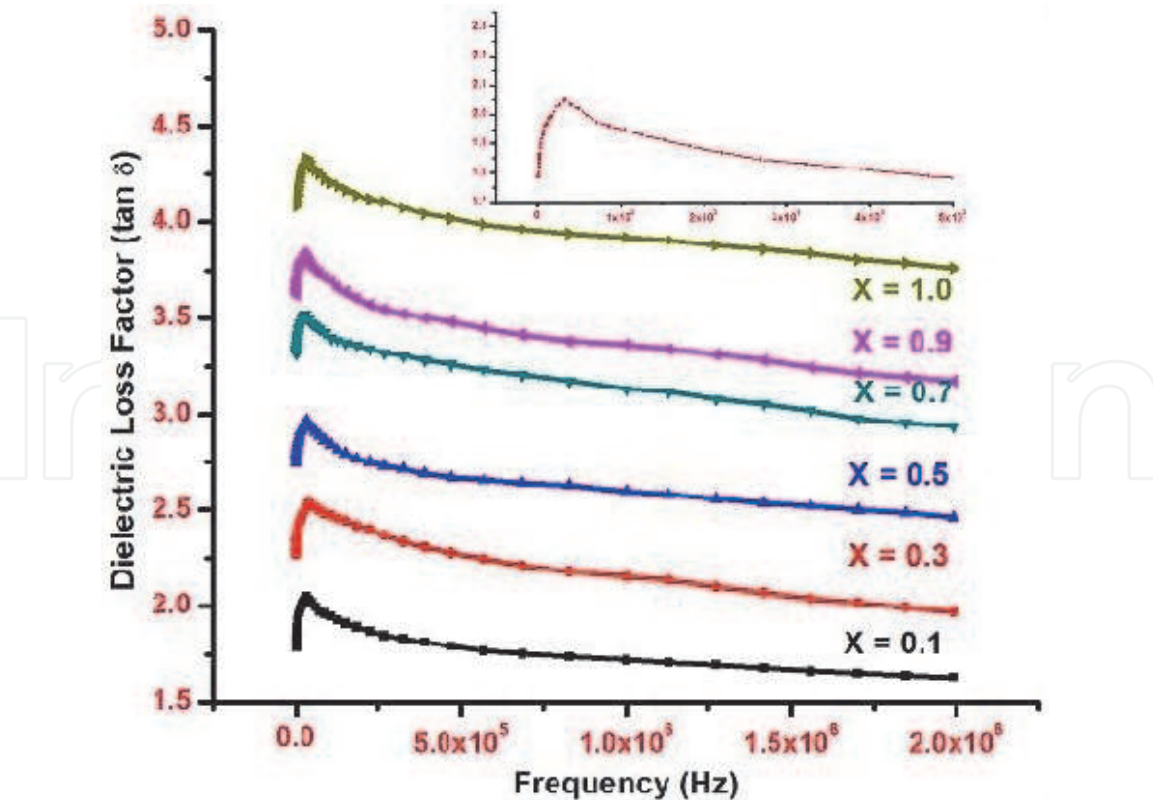


Figure 17.
Dielectric loss tangent ($\tan\delta$) variation of Ni-Cr nano ferrites with frequency.

the frequency of the applied field [80]. Similar type of variation is reported by other researchers [81, 82]. It is clear that at low frequency region dielectric loss decreases sharp and at high frequency region the rate of decrease is slow and it almost frequency independent behavior. A similar trend was observed in case of mixed Ni-Cu nano ceramic system for $X = 0.4, 0.5, 0.8$ and 1.0 under presents investigation. The decrease in $\tan\delta$ with an increase in frequency may be explained on the basis of Koop's phenomenological model.

The AC conductivity variation with frequency is represented in **Figure 18**. It is clear that with increasing frequency ac conductivity increases at low frequency and at high frequency almost independent behavior. This behavior is like to Maxwell-Wagner type [75, 76] in good agreement with Koop's phenomenological theory [77]. According to Koop's phenomenological theory, at lower frequencies region majority are grain boundaries and they act as interference for mobility of charge carriers, hence the hopping electrons between Fe^{2+} and Fe^{3+} ions is less, so conductivity is less. At higher frequency region the conductive grains which become more active and promote the hopping electrons between Fe^{2+} and Fe^{3+} ions, hence the conductivity is more and they are take part for creating charge carriers, these charge carriers are responsible for increasing the ac conductivity. It is in good agreement with the other reports [83, 84].

Dielectric parameter variation with Cr^{3+} ion composition at frequencies 2 MHz are reported in **Table 7**. The dielectric parameters are increases with increase Cr^{3+} ion concentration. The dielectric constant and the AC conductivity reach maximum values at $X = 0.5$ and the loss factor maximum at $X = 0.7$ further increase in Cr^{3+} ion concentration these parameters are decreases. It is due to the formation of Fe^{3+} ions at octahedral sites and it explained with dielectric polarization which is similar to the conduction mechanism in ferrites. Cr ions prefer the octahedral site until the Cr concentration becomes greater than 50% , thereafter Cr ions may increase in tetrahedral sites causing migration of equal number of ions to the octahedral sites [85]

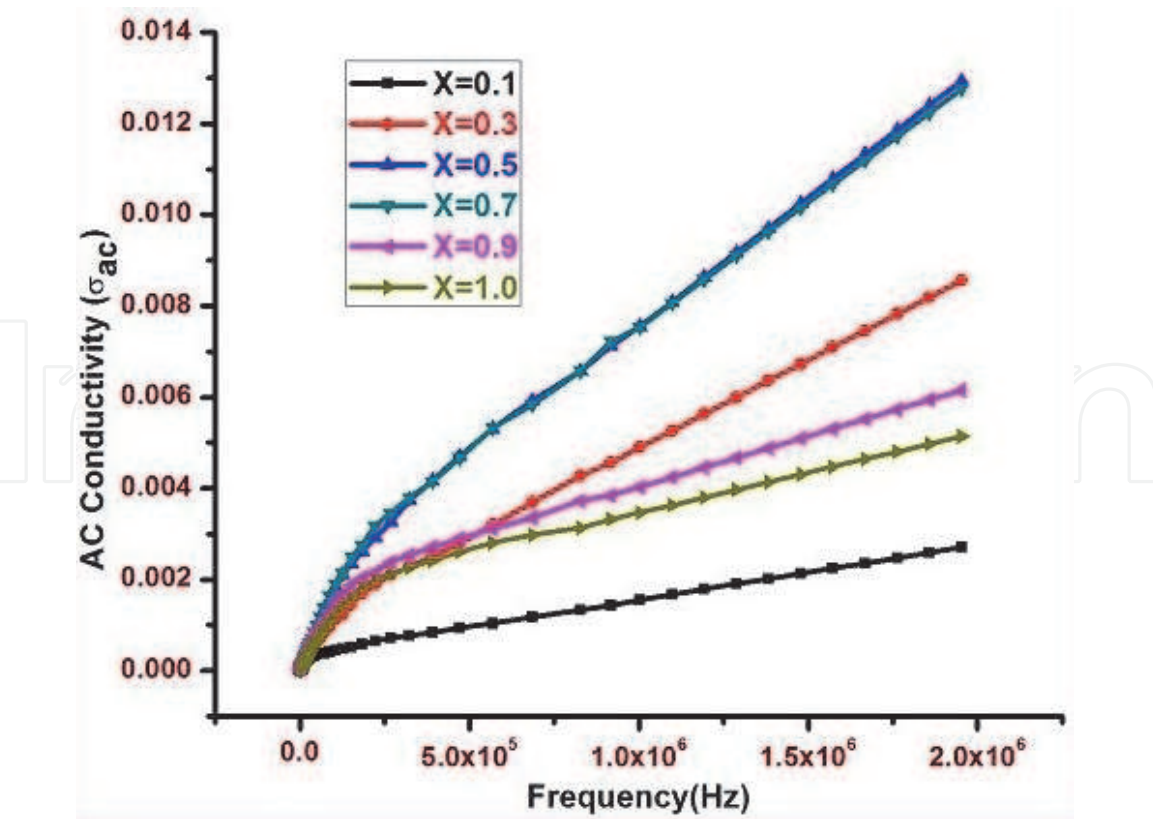


Figure 18. AC conductivity (σ_{ac}) variation of Ni-Cr nano ferrite system with frequency at different frequency.

Sr.No.	Cr content (x)	Dielectric parameters at frequency of 2 MHz		
		ϵ'	$\tan \delta$	σ_{ac}
1	0.1	11.850	1.537	2.70×10^{-03}
2	0.3	17.861	1.608	8.56×10^{-03}
3	0.5	31.243	1.812	1.29×10^{-02}
4	0.7	28.650	2.237	1.28×10^{-02}
5	0.9	4.643	2.044	6.15×10^{-03}
6	1.0	4.166	1.714	5.14×10^{-03}

Table 7. Dielectric parameters of mixed Ni-Cr nano ferrite system.

and decreasing the Fe^{3+} ions at octahedral site there is a least possibility of electronic exchange interaction between Fe^{2+} and Fe^{3+} ions, hence decrease in dielectric parameters with increase in Cr concentration. Similar behavior reported by Raghasudha et al. [86].

4. Conclusions

- The Citrate-gel auto combustion technique is convenient, more efficient and economical for synthesis of investigated nano-cermics.
- X-ray diffraction analysis confirms the single phase cubic spinel structure without impurity peak. From X-ray diffraction analysis data found that the

crystallite size was in range of 8.5–10.5 nm, which indicates the nanocrystalline form.

- In mixed Ni-Cr nano ceramic system the lattice parameter and the hopping length at tetrahedral and octahedral sites are slightly decreases with Cr^{3+} ion dopant. It is due to difference between ionic radii of Fe^{3+} (0.067Å) and Cr^{3+} (0.064Å) ions and it indicating that the systems are obeys Vegard's law.
- In mixed Ni-Cr nano ceramic system increases in X-ray density, porosity and decrease in bulk density with increases in Cr^{3+} ion dopent in Ni nano ceramic. This is due to the atomic weight and density of Fe^{3+} (55.847gram/mole, 7.874gram/cc) more than that Cr^{3+} (51.996gram/mole, 7.14gram/cc).
- Microstructure of mixed Ni-Cr nano ceramic system the existing of Ni, Cr, Fe and O only. The TEM pictures confirm the crystallite formation in nano size.
- FT-IR absorption spectra of the mixed Ni-Cr nano ceramic system revealed the presence of two significant absorption bands around at 600 cm^{-1} and 400 cm^{-1} and it confirms spinel structure in single phase with two sub lattices.
- The saturation magnetization and magnetic moment decreases and the Y–K angles increase with increase Cr^{3+} ion concentrations in Ni nano ceramic. Since the fact that less magnetic moment Cr^{3+} ions ($\sim 3\mu_B$) are substituted in the place of higher magnetic moment Fe^{3+} ions ($\sim 5\mu_B$) at octahedral sublattice site.
- Temperature dependent of dc resistivity shows decreasing trend that suggest the mixed Ni-Cr nano ceramic systems are shown semiconductor behavior. At room temperature resistivity is low and it increases and conductivity decreases with the increase of Cr^{3+} ion concentration. It explains with conduction mechanism between $\text{Fe}^{2+} \leftrightarrow \text{Fe}^{3+}$ ions.
- Prepared samples resistivity is high, which show the way to low eddy current losses are desirable as core materials in electronic applications such as electronic inductors, power transformers, electromagnets and in telecommunication applications.
- The activation energy increases with Cr^{3+} ion concentration increases in Ni nano ceramic. It shows low conductivity of the ceramics goes hand with high activation energy, vice versa.
- Drift mobility of mixed Ni-Cr nano ceramic system has increases with increase in temperature. At room temperature the drift mobility decreases with increases Cr^{3+} concentration. It explain that with higher resistivity have lower mobility and vice versa. It shows the materials are good choice for high frequency applications.
- The Curie temperature (T_c) decreases from 775.39–635.34 K with increase in Cr^{3+} concentration. The Curie temperature (T_c) is good agreement which is measured form Loria-Sinha technique.
- Frequency dependent dielectric measurements such as dielectric constant, loss tangent and ac conductivity results are shows normal dispersion with frequency in Ni-Cr nano ceramic system.

- For all prepared samples the value of $\tan\delta$ exhibits maximum between 1×10^3 - 4×10^4 Hz and further decrease by increasing the frequency and ac conductivity increase with frequency dependent.
- In prepared ceramic systems dielectric loss is low at higher frequencies and conductivity value is low. Hence these ceramic compositions are shows the potential applications like high frequency micro wave devices and in microwave applications.

Author details

Rapolu Sridhar¹, D. Ravinder^{2*}, J. Laxman Naik², K. Vijaya Kumar³, N. Maramu⁴ and S. Katlakunta⁵

¹ Department of BS&H, Vignan Institute of Technology and Science, T.S. State, India

² Department of Physics, Osmania University, Hyderabad, Telangana State, India


³ Department of Physics, JNTUH College of Engineering Sultanpur, Telangana State, India

⁴ Department of Physics, Kakatiya Institute of Technology and Science, Telangana, India

⁵ Department of Physics, University College of Science, Saifabad, Osmania University, Hyderabad, Telangana, India

*Address all correspondence to: ravindergupta28@rediffmail.com

IntechOpen

© 2021 The Author(s). Licensee IntechOpen. This chapter is distributed under the terms of the Creative Commons Attribution License (<http://creativecommons.org/licenses/by/3.0>), which permits unrestricted use, distribution, and reproduction in any medium, provided the original work is properly cited. 

References

- [1] Z. Gao, B. Xu, M. Ma, A. Feng, Y. Zhang, X. Liu, Z. Jia and G. Wu. Electrostatic self-assembly synthesis of ZnFe₂O₄ quantum dots (ZnFe₂O₄@C) and electromagnetic microwave absorption Composites. Part B 2019; 179 107417. <https://doi.org/10.1016/j.compositesb.2019.107417>
- [2] Noppakum Sanpo, James Wang and Christopher C. Berndt. Influence of Chelating Agents on the Microstructure and Antibacterial Property of Cobalt Ferrite Nanopowders. *Journal of Austr. Cer. Soc.*, 2013; 49 84-91. www.austceram.com/ACS-Journal
- [3] Ch.Venkateshwarlu, Ch.Ashok, B. AppaRao, D.Ravinder, B.S.Boyanov. Electrical conductivity of Co–Zr substituted hexagonal barium ferrites. *Journal of Alloys and Compounds* 2006; 426(4) 1-3. <https://doi.org/10.1016/j.jallcom.2006.02.001>
- [4] R. M. Borade, S. B. Somvanshi, S. B. Kale, R. P. Pawar and K. Jadhav. Influence of trivalent Cr ion substitution on the physicochemical, optical, electrical, and dielectric properties of sprayed NiFe₂O₄ spinel-magnetic thin films. *Mater. Res. Express* 2020; 7 016116. <https://doi.org/10.1039/D0RA04319B>
- [5] Kharat, P.B., More, S.D., Somvanshi, S.B. *et al.* Exploration of thermo-acoustics behavior of water based nickel ferrite nanofluids by ultrasonic velocity method. *J Mater Sci: Mater Electron* 2019; 30 6564–6574. <https://doi.org/10.1007/s10854-019-00963-4>
- [6] A. Abou-Hassan, S. Neveu, V. Dupuis and V. Cabuil. Synthesis Of Cobalt Ferrite Nanoparticles In Continuous-Flow Microreactors. *RSC Adv.*, 2012; 2 11263–11266. <https://doi.org/10.1039/C2RA21799F>
- [7] M. Babrekar and K. Jadhav. Synthesis and Characterization of Spray Deposited Lithium Ferrite Thin Film, *Int. Res. J. Sci. Eng.*, 2017; 73–76. <http://www.irjse.in>
- [8] Manik Gupta, B.S. Randhawa. Microstructural, magnetic and electric properties of mixed Cs–Zn ferrites prepared by solution combustion method, *Solid State Sciences*. 2012; 14 849-856. <https://doi.org/10.1016/j.solidstatesciences.2012.04.010>
- [9] H. J. Kardile, S. B. Somvanshi, A. R. Chavan, A. A. Pandit and K. M. Jadhav. Effect of Cd²⁺ doping on structural, morphological, optical, magnetic and wettability properties of nickel ferrite thin films. *Optik*, 2010; 207 164462. <https://doi.org/10.1016/j.ijleo.2020.164462>
- [10] Q. Yue, C. Liu, Y. Wan, X. Wu, X. Zhang and P. Du. Defect engineering of mesoporous nickel ferrite and its application for highly enhanced water oxidation catalysis. *J. Catal.*, 2018; 358 1–7. <https://doi.org/10.1016/j.jcat.2017.10.027>
- [11] R. Zhang, M. Liu, L. Lu, S.-B. Mi and H. Wang. Ultra-low temperature epitaxial growth of lithium ferrite thin films by high-pressure sputtering. *Cryst Eng comm.*, 2015; 17 8256–8263. <https://doi.org/10.1039/C5CE01477H>
- [12] V. Sepel_ak, K. Baabe, K. Mienert, K. Schultze, F. Krumeich, F.J. Litterst, K.D. Becker. Mater Evolution Of Structure And Magnetic Properties With Annealing Temperature In Nanoscale High-Energy-Milled Nickel Ferrite. *J. Magn. Magn.*, 2003; 257 377-386. [https://doi.org/10.1016/S0304-8853\(02\)01279-9](https://doi.org/10.1016/S0304-8853(02)01279-9)
- [13] Pavlović, M., Jovalekić, Č., Nikolić, A.S. *et al.* Mechanochemical synthesis of stoichiometric MgFe₂O₄ spinel. *J Mater Sci: Mater Electron*, 2009; 20 782–787. <https://doi.org/10.1007/s10854-008-9802-2>

- [14] K.M. Batoo, S. Kumar, C.G. Lee, Alimuddin. Study of ac impedance spectroscopy of Al doped $\text{MnFe}_{2-2x}\text{Al}_{2x}\text{O}_4$. *J. Alloys Comp.* 2009; 480 596-602. <https://doi.org/10.1016/j.jallcom.2009.01.137>
- [15] U. Erb. Electrodeposited Nanocrystals: Synthesis, properties and industrial applications. *Nanostructured Materials* 1995; 6(5) 533-538. [https://doi.org/10.1016/0965-9773\(95\)00114-X](https://doi.org/10.1016/0965-9773(95)00114-X)
- [16] M. Pal and D. Chakravorty. Nanocrystalline magnetic alloys and ceramics, *Sadhana. Indian Academy of Sciences* 2003; 28(1-2) 283-297. <https://doi.org/10.1007/BF02717138>
- [17] J. Chargles, N. O'Connor, E. Kolesnichenko, C. Carpenter, S. W. Zheu, A. Kumbhar, S. Jessica and A. Fabrice. *Synthetic Metals*, 2001; 122(3) 547-557. [https://doi.org/10.1016/S0379-6779\(01\)00328-9](https://doi.org/10.1016/S0379-6779(01)00328-9)
- [18] C. Caizer and M. Stefanescu. Magnetic characterization of nanocrystalline Ni-Zn ferrite powder prepared by the glyoxylate precursor method. *Journal of Physics D: Applied Physic*, 2002; 35(23) 3035-3040. <https://doi.org/10.1088/0022-3727/35/23/301>
- [19] A. Dias. Microstructural evolution of fast-fired nickel-zinc ferrites from hydrothermal nanopowders. *Materials Research Bulletin* 2000; 35(9) 1439-1446. [https://doi.org/10.1016/S0025-5408\(00\)00337-8](https://doi.org/10.1016/S0025-5408(00)00337-8)
- [20] S. Gubbala, H. Nathani, K. Koizol and R. D. K. Misra. Magnetic properties of nanocrystalline Ni-Zn, Zn-Mn, and Ni-Mn ferrites synthesized by reverse micelle technique. *Physica B Condensed Matter* 2004; 348(1-4) 317- 328. <https://doi.org/10.1016/j.physb.2003.12.017>
- [21] Liu. Y., Liu. Z., Yang. Y., Yang. H., Shen. G., Yu. R. Sens. synthesis of MgFe_2O_4 Nanoparticles As Gas Sensing Materials. *Actuators. B Simple* 2005; 107 600-604. <https://doi.org/10.1016/j.snb.2004.11.026>
- [22] A. Chatterjee, D. Das, S. K. Pradhan, D. Chakravarty. Synthesis of nanocrystalline Ni-Zn ferrite by the sol-gel method. *Journal of Magnetism and Magnetic Materials* 1993; 127(1-2) 214-218. [https://doi.org/10.1016/0304-8853\(93\)90217-P](https://doi.org/10.1016/0304-8853(93)90217-P)
- [23] A. Pradeep, C. Thangasamy, G. Chandrasekaran. Synthesis and structural studies on $\text{Ni}_{0.5+x}\text{Zn}_{0.5}\text{Cu}_x\text{Fe}_{2-2x}\text{O}_4$, *J. Mater.* 2004; 15 797-802. <https://doi.org/10.1023/B:JMSE.0000045302.52854.0b>
- [24] B. P. Jacob, S. Thankachan, S. Xavier, E. M. Mohammed. Dielectric behavior and AC conductivity of Tb^{3+} doped $\text{Ni}_{0.4}\text{Zn}_{0.6}\text{Fe}_2\text{O}_4$ nanoparticles. *Journal of Alloy of Compounds* 2012; 541 29-35. <https://doi.org/10.1016/j.jallcom.2012.07.033>
- [25] Chen. N.S., Yang. X.J., Liu. E.S., Huang. J.L., Sensors and Actuators B: Chemical Reducing gas-sensing properties of ferrite compounds MFe_2O_4 (M=Cu, Zn, Cd and Mg). 2000; 66 178. [https://doi.org/10.1016/S0925-4005\(00\)00368-3](https://doi.org/10.1016/S0925-4005(00)00368-3)
- [26] S. B. Kale, S. B. Somvanshi, M. N. Sarnaik, S. D. More, S. J. Shukla and K. M. Jadhav. Enhancement in surface area and magnetization of CoFe_2O_4 nanoparticles for targeted drug delivery application. *AIP Conf. Proc.*, 2018; 1953 030193. <https://aip.scitation.org/doi/abs/10.1063/1.5032528>
- [27] M. Kaiser. Electrical conductivity and complex electric modulus of titanium doped nickel-zinc ferrites. *Physica B* 2012; 407 606. <https://doi.org/10.1016/j.physb.2011.11.043>
- [28] A. M. Abdeen, O.M. Hemeda, E.E. Assem, M.M.El-Sehly. Structural, electrical and transport phenomena of Co ferrite substituted by Cd. *Journal of*

Magnetism and Magnetic Materials 2002; 238 75-83. [https://doi.org/10.1016/S0304-8853\(01\)00465-6](https://doi.org/10.1016/S0304-8853(01)00465-6)

[29] S. B. Somvanshi, R. V. Kumar, J. S. Kounsalye, T. S. Saraf and K. M. Jadhav. Investigations of structural, magnetic and induction heating properties of surface functionalized zinc ferrite nanoparticles for hyperthermia applications. *AIP Conf. Proc.*, 2019; 2115 030522. <https://doi.org/10.1063/1.5113361>

[30] A. R. Chavan, R. R. Chilwar, P. B. Kharat and K. Jadhav. Impact of Trivalent Metal Ion Doping on Structural, Photoluminescence and Electric Properties of NiFe_2O_4 Thin Films. *J. Supercond.*, 2018; 1–10. <https://doi.org/10.1007/s11664-019-07329-w>

[31] D. R. Mane, D. D. Birajdar, Sagar E. Shirsath, R. A. Telugu, R. H. Kadam. Structural and magnetic characterizations of $\text{Ni}_{0.7-x}\text{Mn}_x\text{Zn}_{0.3}\text{Fe}_2\text{O}_4$ ferrite nanoparticles. *Physica Status Solidi (a)* 2010; 207 2355–2363. <https://doi.org/10.1002/pssa.201026079>

[32] M. A. Gabal, Y. M. Al Angari and S. S. Al-Juaied. A study on Cu substituted Ni–Cu–Zn ferrites synthesized using egg-white. *Journal of Alloys and Compounds* 2010; 492(1-2) 411-415. <https://doi.org/10.1016/j.jallcom.2009.11.124>

[33] S. S. Bellad, R. B. Pujar, B. K. Chougule. Structural and magnetic properties of some mixed Li-Cd ferrites. *Materials Physics and Chemistry* 1998; 52 166-169. [https://doi.org/10.1016/S0254-0584\(98\)80019-9](https://doi.org/10.1016/S0254-0584(98)80019-9)

[34] C.B.Kolekar, P.N.Kumble and S.G. Kulkarni. Effect of Gd^{3+} substitution on dielectric behavior of copper-cadmium ferrites, *Journal of Materials Science*. 1995; 30 (22) 5784-5788. <https://doi.org/10.1007/BF00356721>

[35] A. R. Chavan, M. Babrekar, A. C. Nawle and K. Jadhav. Structural and Optical Properties Of Nanocrystalline Ni–Zn Ferrite Thin Films. *J. Electron. Mater.*, 2019; 48 5184–5194. <https://doi.org/10.1016/j.jallcom.2010.07.171>

[36] N.F. Mott, E.A. Davis. *Electron4. IC Processes in Non-crystalline Material*. Oxford, London. 1979;

[37] S. M. Hoque, Md. A. Choudhury, Md. F. Islam. Characterization of Ni-Cu mixed spinel ferrite. *Journal of Magnetism and Magnetic Materials* 2002; 251 292-303. [https://doi.org/10.1016/S0304-8853\(02\)00700-X](https://doi.org/10.1016/S0304-8853(02)00700-X)

[38] V. Vinayak, P. P. Khirade, S. D. Birajdar, R. Alange and K. Jadhav. Electrical and Dielectrical Properties of Low-Temperature-Synthesized Nanocrystalline Mg^{2+} -Substituted Cobalt Spinel Ferrite Novel. *Magn., J. Supercond.*, 2015; 28 3351–3356. <https://doi.org/10.1007/s10948-015-3159-6>

[39] P. K. Gupta, C.T. Hung. Magnetically controlled targeted micro-carrier systems. *Life Sciences*. 1989; 44 175-186. [https://doi.org/10.1016/0024-3205\(89\)90593-6](https://doi.org/10.1016/0024-3205(89)90593-6)

[40] Devan, R.S., Kolekar, Y.D., Chougule, B.K. Effect of cobalt substitution on the properties of nickel-copper ferrite. *J. Phys., Condens. Matter*. 2006; 18, 9809–9821 <https://iopscience.iop.org/article/10.1088/0953-8984/18/43/004>

[41] L. Vergard. “Die Konstitution der Mischkristalle, Die Raumfüllung der Atome” *Physik A: Had- rons and Nuclei*. 1921; 5(1) 17-26. <https://doi.org/10.1007/BF01349680>

[42] Compounds, B.I. International Union of Crystallography. Commission on Crystallographic Data List of works containing new data on crystal structures. 1961.. *J Struct Chem*. 1964;

4 739–754. <https://doi.org/10.1007/BF00747673>

[43] J.B. Li, G.H. Rao, J.K. Liang, Y.H. Liu, J. Luo, J.R. Chen. Magnetic properties of $\text{Bi}(\text{Fe}_{1-x}\text{Cr}_x)\text{O}_3\text{Bi}(\text{Fe}_{1-x}\text{Cr}_x)\text{O}_3$ synthesized by a combustion method. *Appl. Phys. Lett.*, 2007; 90 162513. <https://doi.org/10.1063/1.2720349>

[44] S.H. Lee, S.J. Yoon, G.J. Lee, H.S. Kim, C.H. Yo, K. Ahn, D.H. Lee, K.H. Kim. Electrical and magnetic properties of $\text{NiCr}_x\text{Fe}_{2-x}\text{O}_4$ spinel ($0 \leq x \leq 0.6$) *Mater. Chem. Phys.*, 1999; 61 147. [https://doi.org/10.1016/S0254-0584\(99\)00136-4](https://doi.org/10.1016/S0254-0584(99)00136-4)

[45] M. Raghasudha. Characterization of nano-structured magnesium chromium ferrites synthesized by citrate-gel auto combustion method. *Adv. Mat. Lett.*, 2013; 4(12) 910-916. <https://DOI:10.5185/amlett.2013.5479>

[46] Muhammed Javed Iqbal, Mah Rukh Siddiquah. Electrical and magnetic properties of chromium-substituted cobalt ferrite nanomaterials. *J. Alloys Comp.*, 2008; 453 513. <https://doi.org/10.1016/j.jallcom.2007.06.105>

[47] M.A. Gabal, W.A. Bayoumy, A. Saeed, Y.M. Al Angari. Structural And Electromagnetic Characterization Of Cr-Substituted Ni–Zn Ferrites Synthesized Via Egg-White Route. *Journal of Molecular Structure.*, 2015; 1097 45–51. <https://doi.org/10.1016/j.molstruc.2015.04.032>

[48] R. D. Waldron. Infrared Spectra of Ferrites. *Physical Review of Journals Archive*. 1955; 99 1727. <https://link.aps.org/doi/10.1103/PhysRev.99.1727>

[49] R.M. Mohamed, M.M. Rashad, F.A. Haraz, W. Sigmund. Structure and magnetic properties of nanocrystalline cobalt ferrite powders synthesized using organic acid precursor method. *J. Magn. Magn. Mater.*, 2010; 322 2058. <https://doi.org/10.1016/j.jmmm.2010.01.034>

[50] Rintu Mary Sebastian, Sheena Xavier. E M Mohammed. Structural and electrical studies of Gd^{3+} substituted zinc ferrite nano particles. *IJESIT*. 2013; 2 4. <https://doi.org/10.1080/00150193.2016.1239478>

[51] S.A. Mazen And A.M. Abdel-Daiem. IR Spectra And Dielectric Properties Of Cu–Ge Ferrite. *Mater. Chem. Physics*, 2011; 130 847-852. <https://doi.org/10.1016/j.matchemphys.2011.09.017>

[52] Santosh Bhukal, Tsering Namgyal, S. Mor, S. Bansal, Sonal Singhal. Structural, electrical, optical and magnetic properties of chromium substituted Co–Zn nanoferrites $\text{Co}_{0.6}\text{Zn}_{0.4}\text{Cr}_x\text{Fe}_{2-x}\text{O}_4$ ($0 \leq x \leq 1.0$) prepared via sol–gel auto-combustion method. *Journal of Molecular Structure*. 2012; 1012 162–167. <https://doi.org/10.1016/j.molstruc.2011.12.019>

[53] Y.M. Yokovlev, L.B. Rubarikaya, N. Lapovok, Sov. Magnetic and electrical properties of Cr substituted Ni nano ferrites. *Phys.Solid.State.*, 1969; 10 2301. <https://doi.org/10.2298/PAC1801001V>

[54] S. Chikazumi. Physics of Magnetism. Wiley. New York. 1959;

[55] M. George, A.M. John, S.S. Nair, P. A. Joy, M.R. Anantharaman. Finite size effects on the structural and magnetic properties of sol–gel synthesized NiFe_2O_4 powders. *J. Magn. Magn. Mater.*, 2006; 302 190–195. <https://doi.org/10.1016/j.jmmm.2005.08.029>

[56] F. Li, H. Wang, L. Wang, J. Wang. Magnetic properties of ZnFe_2O_4 nanoparticles produced by a low - temperature solid-state reaction method. *J. Magn. Magn. Mater.*, 2007; 309 295. <https://doi.org/10.1016/j.jmmm.2006.07.012>

[57] Y. Koseoglu, H. Kavas. Size and Surface Effects on Magnetic Properties of Fe_3O_4 Nanoparticles. *J. Nanosci. Nanotechnol.*, 2008; 8 584. <https://doi.org/10.1166/jnn.2008.B012>

- [58] Y. Yafet, C. Kittel. Physical Review. 1952; 87 239.
- [59] A.K. Ghatage, S.C. Choudhary, S.A. J. Patil. Mater. X-ray, Structure and magnetic properties of Cd and Ti/Si substituted cobalt ferrites. *Sci. Lett.*, 1996; 15 1548–1550. [https://doi.org/10.1016/S0254-0584\(98\)00202-8](https://doi.org/10.1016/S0254-0584(98)00202-8)
- [60] E.J.W. Verwey. The Crystal Structure of γ -Fe₂O₃ and γ -Al₂O₃. *Z. Kristallogr, Kristallgeo.* 1935; 91 65. <https://doi.org/10.1524/zkri.1935.91.1.65>
- [61] M.J. Iqbal, M.R. Siddiquah. Structural, electrical and magnetic properties of Zr–Mg cobalt ferrite. *J. Magn. Magn. Mater.*, 2008; 320 845–850. <https://doi.org/10.1016/j.jmmm.2007.09.009>
- [62] Sagar E. Shirsath, B.G. Toksha, Maheshkumar L. Mane, V.N. Dhage. Frequency, temperature and In³⁺ dependent electrical conduction in NiFe₂O₄ powder. *Powder Technology.*, 2011; 212 218–223. <https://doi.org/10.1016/j.powtec.2011.05.019>
- [63] R. Manjula, V.R.K. Murthy, J. Sobhanadri. Electrical conductivity and thermoelectric power measurements of some lithium–titanium ferrites. *J. Appl. Phys.*, 1986; 59 2929. <https://doi.org/10.1063/1.336954>
- [64] S.M. Patange, Sagar E. Shirsath, B. G. Toksha, S.S. Jadhav, K.M. Jadhav. Electrical and magnetic properties of Cr³⁺ substituted nanocrystalline nickel ferrite. *J. Appl. Phys.*, 2009; 106 023914-1. <https://doi.org/10.1063/1.3176504>
- [65] S.M. Ramay, S.A. Siddiqi, S. Atiq, M. S. Awan, S. Riaz, Chin. Structural, Magnetic, and Electrical Properties of Al³⁺ Substituted CuZn-ferrites. *J. Chem. Phys.*, 2010; 23 591–595. DOI:10.1088/1674-0068/23/05/591-595
- [66] M. Azhar Khan, M.U. Islam, M. Ishaque, I.Z. Rahman. Effect of Tb substitution on structural, magnetic and electrical properties of magnesium ferrites. *Ceramics International.*, 2011; 37 2519–2526. <https://doi.org/10.1016/j.ceramint.2011.03.063>
- [67] N. Rezlescu, E. Rezlescu, P.D. Popa, L. Rezlescu. Effects of rare-earth oxides on physical properties of Li–Zn ferrite. *Journal of Alloys and Compounds.*, 1998; 657–659. [https://doi.org/10.1016/S0925-8388\(98\)00413-7](https://doi.org/10.1016/S0925-8388(98)00413-7)
- [68] A.B. Gadkari, T.J. Shinde, P.N. Vasmbekar. Structural analysis of Y³⁺-doped Mg–Cd ferrites prepared by oxalate co-precipitation method, Materials Chemistry and Physics. 2009; 114 505–510. <https://doi.org/10.1016/j.matchemphys.2008.11.011>
- [69] B. Ramesh, D. Ravinder. Electrical properties of Li–Mn ferrites. *Materials Letters*, 2008; 62 2043–2046. <https://doi.org/10.1016/j.matlet.2007.11.010>
- [70] Santosh Bhukal, Tsering Namgyal, S. Mor, S. Bansal. Structural, electrical, optical and magnetic properties of chromium substituted Co–Zn nanoferrites Co_{0.6}Zn_{0.4}Cr_xFe_{2–x}O₄ (0 ≤ x ≤ 1.0) prepared via sol–gel auto-combustion method. *Journal of Molecular Structure*, 2012; 1012 162–167. <https://doi.org/10.1016/j.molstruc.2011.12.019>
- [71] Muhammad Naeem Ashiq, Farah Naz, Muhammad Aslam Malana, R S Gohar. Role of Co–Cr substitution on the structural, electrical and magnetic properties of nickel nano-ferrites synthesized by the chemical co-precipitation method. *Materials Research Bulletin.*, 2012; 47 683–686. <https://doi.org/10.1016/j.materresbull.2011.12.017>
- [72] A. Lakshman, K.H. Rao, R.G. Mendiratta. Magnetic properties of In³⁺ and Cr³⁺ substituted Mg–Mn ferrites. *J. Magn. Magn. Mater.*, 2002; 250 92–97. [https://doi.org/10.1016/S0304-8853\(02\)00359-1](https://doi.org/10.1016/S0304-8853(02)00359-1)

- [73] S.J. Haralkar, R.H. Kadam, S.S More, Sagar E. Shirsath, M.L. Mane, Swati Patil. Substitutional effect of Cr^{3+} ions on the properties of Mg–Zn ferrite nanoparticles. *Physica B*. 2012; 407 4338–4346. <https://doi.org/10.1016/j.physb.2012.07.030>
- [74] Chandra Babu B, Naresh V, Jayaprakash B, Buddhudu S. Structural, thermal and dielectric properties of lithium zinc silicate ceramic powders by sol-gel method. *Journal of ferroelectric letters section*. 2011; 38 124-130. <https://doi.org/10.1080/07315171.2011.623610>
- [75] J.C. Maxwell. *Electricity and Magnetism*. Oxford University. Press, London. 1973;.
- [76] K.W.Wagner. *Ann. Phys.* 1993; 40 818.
- [77] C.G. Koops. *Phys. Rev.* 1951; 83 121.
- [78] A.M. Shaikh, S.S. Bellad, B.K. Chougule. Temperature and frequency-dependent dielectric properties of Zn substituted Li–Mg ferrites. *J.Magn. Magn. Mater.*, 1999; 195 384-390. [https://doi.org/10.1016/S0304-8853\(99\)00138-9](https://doi.org/10.1016/S0304-8853(99)00138-9)
- [79] I.T. Rabinkin, Z.I. Novikova, Ferrites, *Izv Acad. Nauk USSR Minsk*. 1960; 146.
- [80] N. Rezlescu and E. Rezlescu. Dielectric properties of copper containing ferrites. *Phys. Status Solidi A*, 1974; 23 575-582. <https://doi.org/10.1002/pssa.2210230229>
- [81] R.K.Kotnala, M.Abdullah Dar, Vivek Verma, A.P.Singh. Synthesis and characterizations of Ni^{2+} substituted cobalt ferrite nanoparticles. *Journal of Magn. Magn. Matter*. 2010; 322 3714-3719. <https://doi.org/10.1016/j.matchemphys.2012.09.019>
- [82] Mohd Hashim, Alimuddin, Sagar E. Shirsath, Shalendra Kumar, Ravi Kumar. Preparation and characterization chemistry of nano-crystalline Ni–Cu–Zn ferrite. *Journal of Alloys. Comp.*, 2013; 549 348-357. <https://doi.org/10.1016/j.jallcom.2012.08.039>
- [83] R. M. Sebastian. Structural and dielectric studies structural and dielectric studies tural and dielectric studies of Cr^{3+} doped znfe doped znfe_2O_4 nanoparticles Nano Studies. *Journal_of_Nano_Research*, 2013; 8 121-130. <https://www.researchgate.net/journal/1661-9897>
- [84] M. Raghasudha, D. Ravinder, P. Veerasomaiah. Influence of Cr^{+3} Ion on the Dielectric Properties of NanoCrystalline Mg-Ferrites Synthesized by Citrate-Gel Method. *Materials Sciences and Applications*. 2013; 4 432-438. <https://DOI:10.4236/MSA.2013.47052>
- [85] D. Elkony, Study of dielectric and impedance properties of Mn ferrites. *Egypt J. solids*, 2004; 27 285-296.
- [86] M. Raghasudha, D. Ravinder, P. Veerasomaiah. Electrical and Magnetic Properties of Mg-Cr and Co-Cr Nano Ferrites Synthesized by Citrate-Gel Method. *Solid State Phenomena.*, 2016; 241 69-92. <https://doi.org/10.4028/www.scientific.net/SSP.241.69>